ON THE EVALUATION OF RHEOLOGICAL PROPERTIES OF MEDIA USED IN ABRASIVE FLOW MACHINING (AFM)

by

C. RANGANATHA

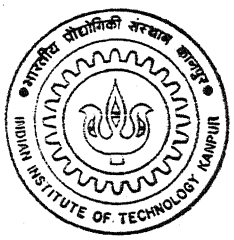

DEPARTMENT OF MECHANICAL ENGINEERING

Indian Institute of Technology Kanpur

OCTOBER, 1997

ON THE EVALUATION OF RHEOLOGICAL PROPERTIES OF MEDIA USED IN ABRASIVE FLOW MACHINING (AFM)

by

C. RANGANATHA

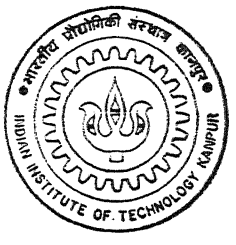

DEPARTMENT OF MECHANICAL ENGINEERING

Indian Institute of Technology Kanpur

OCTOBER, 1997

ON THE EVALUATION OF RHEOLOGICAL PROPERTIES OF MEDIA USED IN ABRASIVE FLOW MACHINING (AFM)

A Thesis Submitted

in Partial Fulfillment of

the Requirements for

the Degree of

MASTER OF TECHNOLOGY

by

C. RANGANATHA

to the

Department Of Mechanical Engineering

INDIAN INSTITUTE OF TECHNOLOGY, KANPUR

October, 1997

ME-1997-M-RAN-EVA

CERTIFICATE

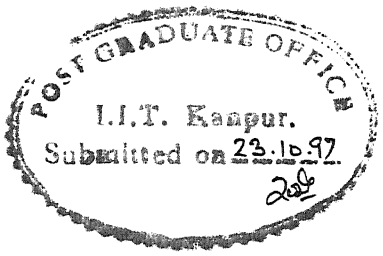

It is certified that the work contained in the thesis entitled " **ON THE EVALUATION OF RHEOLOGICAL PROPERTIES OF MEDIA USED IN ABRASIVE FLOW MACHINING (AFM)**", by Mr. **C. RANGANATHA,** has been carried out under my supervision and this work has not been submitted elsewhere for a degree.

October, 1997

Dr. V. K. Jain,
Professor,
Dept. of Mechanical Engg.
I.I.T. Kanpur.

ABSTRACT

Abrasive Flow Machining (AFM) is a new non-traditional machining process used to deburr, radius, polish and remove recast layers of components in a wide range of applications. The material removal in AFM takes place by flowing the media (i.e carrier like putty) mixed with abrasives, across the surface to be machined. The media is the key element in the process because of its ability to precisely abrade the selected areas along its flow path. From the literature review, it is found that there is a need to study the media property, i.e. viscosity of the media which has significant effect on the process performance parameters.

In the present work, the effects of concentration and mesh size of abrasives, and its temperature on viscosity have been studied. To determine the viscosity of the abrasive media, the viscometer set-up has been fabricated based on the principle of capillary viscometry. Experiments have been conducted at different concentration, mesh sizes and temperatures. It is observed from the experimentation that the viscosity of the media increases with % concentration and decreases with the mesh size and temperature. Experimental and theoretical values (obtained from the mathematical model) are compared and presented. The most dominating factor that is effecting the viscosity of the media is % concentration of abrasives followed by mesh size and temperature. The results of viscosity are then correlated with the process performance parameters, i.e. material removal and surface roughness. It is observed that there is an increase in the material removal and decrease in the surface roughness values as the viscosity of the media increases.

ACKNOWLEDGMENTS

I take this opportunity to express the feeling of sincere gratitude towards my thesis supervisor Dr. V.K. Jain for his expert guidance, and encouragement, which have been vital factors in successful completion of the present work. I am very thankful to Dr. K. Muralidhar for his guidance in viscosity measurements.

I am very grateful to the staff of manufacturing science laboratory, Mr. R.M. Jha, Mr. Namdev, Mr. Sharma, Mr. P.N. Mishra and Mr. B.P. Bharatiya for their help in preparing the experimental set-up.

I am very thankful to Mr. R.K. Jain and Mr. Santosh kumar for their encouragement, suggestions and criticism. I am very thankful to my friends Kishore, M.S. Reddy, Appaji Rao, Seshu, Murthy, Master, Narendra, Rajani kumar, Siva rama krishna who made my stay in I.I.T most memorable and enjoyable. I also take this opportunity to thank my class mates and other friends.

C. RANGANATHA

DEDICATED

TO

MY PARENTS

NOMENCLATURE

A	Area of cross-section of the tube (m^2)
b	constant
d_g	Size of abrasive particle (mm)
F_v	Viscous force (N)
L	Length of the tube (m)
m	Mesh size
MT_s	Media temperature at the side surface of the tube (^0C)
MT_c	Media tempeature at the core (^0C)
$\bar{L}$	Average length of the media in the tube (m)
p	Pressure drop across the capillary (N/m^2)
$\frac{p}{L}$	Pressure gradient across the capillary (N/m^3)
Q	Volumetric flow rate (m^3/sec)
R	Radius of the tube (m)
R_a	Surface roughness (μm)
t	time interval (min)
u	Axial velocity along the tube (m/sec)
w	Weight applied on the media (kg)

ΔT	Temperature rise in ^{0}C
Δv	Voltage difference in mV
γ	Apparent shear rate (s^{-1})
η_a	Apparent viscosity (kN-s/m^2)
η_{pl}	Plastic viscosity (kN-s/m^2)
τ	Shear stress (kN/m^2)
τ_w	Shear stress at the wall (kN/m^2)
ψ	Yield stress (kN/ m^2)

CONTENTS

LIST OF FIGURES

LIST OF TABLES

Chapter 1

INTRODUCTION

1.1 Traditional finishing processes

Machining of precision parts involves labour intensive finishing operations that frequently absorb as much as 15% of the total manufacturing cost. These final machining operations are uncontrollable and if they are not carried out properly, performance of the machined component may be far from optimum. The dimensional and alignment accuracy, and the quality of the surface finish are taken care of by finishing processes. Grinding, lapping, honing and superfinishing are *traditional methods* of finishing. Grinding provides surface irregularities between 0.1 to 5 μm, honing between 0.025 to 0.4 and lapping between 0.012 to 0.16 μm.

Grinding is a finishing process in which work is fed against the rotating wheel or cutting tool to remove the material. The material removal during grinding depends upon the factors like abrasive size, abrasive type, bond of the wheel, structure of the wheel, work speed, wheel speed, machining conditions etc. Generally grinding is used to remove more stock of material as compared to other finishing processes. Grinding is generally performed at high speeds, therefore use of coolant is essential to protect the workpiece from thermal deformation. Lapping is a low pressure abrading process, which is used to produce geometrically true surfaces, correct the minor surface imperfections, improve the dimensional accuracy, and to provide a close fit between the two contact surfaces. The material is removed from the surface of workpiece to be

lapped and the lap [Insak et al., 1993] . Abrasive powders such as emery, iron oxide, etc . mixed with oil or pastes as carrier are used in lapping . The important variables affecting lapping efficiency are abrasive grain size, lapping pressure, lapping speed, quantity of lapping compound supplied, etc. [Ghosh and Mallik, 1985].

Honing is the abrading process used for finishing the holes, and also used to correct some 'out-of-roundness', taper, tool marks etc. Honing tool is so made that a floating action between the work and the tool prevails and the pressure is transmitted equally to all the sides. Honing process is characterized by means of abrasive contact, low cutting pressure, low velocity and automatic centering by expanding inside the hole. [Lee and Mallkin, 1993.] .

Superfinishing is an operation which uses abrasive stones in a particular way to produce an extremely high quality surface finish. A very thin layer of material is removed in superfinishing process. The superfinishing is carried out with the appropriately selected abrasives and lubricant. It has proved to be an effective means for removing thin skin left over after grinding, surface tensile stresses and permanent deformation. In order to obtain better finish and to prevent possible loading on the working surface, recommendation is made for the use of porous CBN stones. [Onchi and Mastumori, 1995] . These *fine finishing processes* are being pushed to their limits of performance and productivity in general, in case of harder materials and complicated shapes in particular. The general shapes worked by lapping, honing and superfinishing are limited to basic forms such as flat, cylindrical and spherical. Hence , with the introduction of hard materials, components of complicated shapes and computer

aided manufacturing, there is need to develope an accurate and reliable finishing process with wider range of application areas, better quality performance, and higher productivity. Abrasive flow machining (AFM) is one of such processes.

1.2 Abrasive flow machining (AFM)

Abrasive flow machining (AFM) is a non-traditional finishing process that is used to deburr, polish, radius, remove recast layer and to produce compressive residual stresses. AFM promises to provide accuracy, efficiency, economy and the possibility of effective automation needed . In AFM, workpiece is clamped between the two vertically opposed cylinders and material is removed by flowing the media through restrictive passage formed by work-tool combination [Williams and Rajurkar, 1992].

In AFM, abrasion occurs only in the area where the media flow is restricted. Abrasion can be controlled by two factors namely, depth of cut and number of cuts. Depth of cut primarily depends upon the size, relative hardness and sharpness of abrasive grains, and extrusion pressure. Second factor is controlled by the length of the media slug as it passes through the restriction.

AFM can generate edge radius from less than 0.025 to more than 1.52 mm [Rhoades,1989]. In the first few cycles itself, about 90% of the total improvement in surface finish with minimal dimensional change can be achieved [Kohut Tom, 1989]. AFM promises to provide precision, consistency, flexibility and economy needed for manufacturing. Applications of

this process range from precision medical and aerospace components to high volume production of electronic and automotive components. Other applications have been developed in the areas as diverse as surgical implant and centrifugal pumps. The process was initially developed to perform critical deburring of aircraft valve bodies and spools as well as burr free internal edges [Rhoades, 1989]. Control of edge quality and surface finish can dramatically improve the product performance and its life. Removing stress risers at sharp corners by producing controlled radii on edges can substantially improve thermal and mechanical fatigue strength of highly stressed components.

AFM process can be applied to a wide range of parts and sizes ranging from as small as 0.2 mm orifices to turbine disks of nearly 1.2 m in diameter. AFM can simultaneously process many selected areas on a workpiece including even typically inaccessible areas and complex internal surfaces. Materials from soft aluminium to tough nickel alloys, ceramics and carbides can be successfully micromachined with this process.

In AFM, abrasive action depends upon extrusion pressure, flow volume and flow speed which are determined by machine settings and media formulation which includes media viscosity, abrasive type, size and concentration.

1.3 Literature review

Rhoades [1989] observed that AFM can be applied to achieve a wide range of predictable and repeatable results. The objective of AFM involves

uniformly polishing the walls of the restrictive passages. In case of deburring or radiusing the edges of the passage, a less viscous media can be used, because it has easier flow once it enters the passage and abrades the edges more than the passage walls. The type of flow pattern to occur depends upon the machine settings, media formulation, workpiece and tool configuration.

Przylenk [1986] found that with the increase in the number of cycles, there is initial increase in the stock removal due to high initial coarseness of the workpiece surface, afterwards it slightly decreases. At the beginning and end of the passage, there is increase of the edge radius with the number of cycles. Media viscosity increases with the concentration of abrasives and hence the flow velocity decreases.

Loveless[1994] investigated the effect of initial surface condition (pre-AFM surface condition) achieved by different machining processes. It was found to significantly affect the material removal rate during AFM. It is concluded that found that the amount of material removal from the milled surface is more than that of the WEDM, turned and grounded workpiece surface.

According to Perry [1989] abrasion is high when the velocity is high. Media velocity is inversely proportional to the flow area. If two holes have different diameters but equal flow area, then they will abrade equally. High viscosity media provides high material removal rate and low viscosity media is used for radiusing purpose. Likewise coarse abrasives are used for faster cutting and fine abrasives for flowing through small holes, or for highly polished finishing.

Williams[1992] did some experiments to study the effect of media viscosity and extrusion pressure on the material removal rate and surface finish. The experiments carried out with silicon carbide abrasives having mesh size 70 and concentration 66% by weight. It is observed that the material removal and surface finish in AFM are significantly affected by the media viscosity, extrusion pressure (Fig 1.1(a-d)). Extrusion pressure seems to be highly significant in improving surface finish. SEM photographs of the AFM generated surfaces show that the major improvement in surface finish takes place within the first few cycles[Rhoades, 1989]. It is also found that if the flow volume is held constant, variation in flow rate does not affect significantly the material removal (Fig 1.2).

Kohut Tom [1989] presented some fundamentals of the process. For any working pressure the amount of abrasion that occurs relates directly to the slug length of flow (the medium flow volume divided by the cross-sectional area of the passage). If the two passages of different areas are given the same volume of flow, then the smaller passage abrades more than the larger passage due to greater slug length of flow. If both are processed at the same machining time, the smaller passage will have passed shorter slug length of flow, since it offers more resistance to media flow, yielding less abrasion than the larger passage. If the passage length is substantially shorter than two times the passage width, a higher viscosity media or lower extrusion pressure should be used. Conversely, if the passage length is longer than two times that of the passage width, lower viscosity media or high extrusion pressure is required.

Rajeshwar [1994] presented a mathematical model to determine the characteristics of the media flow during machining. The simulation model is developed using the constitutive equations of Maxwell model describing non-Newtonian flow characteristics of the AFM media through cylindrical workpieces. Finite difference method was used to obtain the solution of constitutive equations. To compare the theoretical values obtained from the simulation model, experiments are carried out on AISI 4140 cylindrical workpiece with diameter 76mm and height 50.8 with initial hole diameters 25mm and 29mm . A 70 grit silicon grit abrasive was used at concentration 37% by weight. characteristics in AFM process. The model is experimentally validated and is observed that there is a linear relationship exits between the shear stress on the surface and thickness of the material removed.

Davies [1996] observed the relationships between rheological behaviour of polyborosiloxane (PBS) grit mixtures and their machining characteristics. The experiments were conducted on three types of polyborosiloxane grit mixtures (i.e. LV, MV, HV) , SiC grit sizes (60 and 100 mesh) and grit-PBS ratios (0,1,2). It is observed from the experimental results that the relationship between number of extrusion cycles and both the temperature and pressure drop depends upon the media type and the grit-PBS ratio. It is found that increase in the temperature results decrease in the viscosity of the media and increase in the volumetric flow rate as shown in Fig.1.5.

Fletcher [1996] experimentally determined the physical properties of the media such as thermal conductivity, specific heat capacity and surface heat transfer coefficient of media. To determine the thermal conductivity , Lees disc

apparatus was used as shown in Fig 1.3. A containment ring was introduced between the hot and cold plates of standard Lees disc apparatus. The containment ring is filled with enough mixture to create a disc of uniform thickness. The thermal conductivity of the mixture was calculated by measuring the temperature across the specimen and using the principle of Fourier equation for conduction. Specific heat capacity of the media was determined by calorimetric method. To determine the surface heat transfer coefficient a special test rig was designed as shown in Fig 1.4 . A steel sheathed heating element was housed concentrically within the steel cylinder and the gap between the two is filled with the mixture of polymer and abrasive. By controlling the voltage applied to the heating element, variable amounts of energy is supplied to the system. Thermocouples were positioned within the system to monitor the thermal response of the system in conjunction with the energy supplied and measured temperature distribution at the equilibrium condition. These experimental values are then validated with the mathematical model of each property, which are then used in the calculation of the thermal behaviour of mixture as a function of material composition and temperature.

From the above literature survey it is evident that the enough work has not been done with regards to the evaluation of the rheological properties of the media used in AFM in general, and the putty-abrasive media in particular. Hence the objective of the present work was set as given below.

1.4 Objectives of present work

The main objectives of the present work are

- Design and fabrication of the set-up for the measurement of viscosity of the media.
- To study how viscosity is changing with the change in abrasive concentration and grit size.
- To study how viscosity is effecting with the shear stress, shear rate and change in temperature.
- To correlate the above results with the process performance results of others particularly those given in ref. [Adsul , 1996]

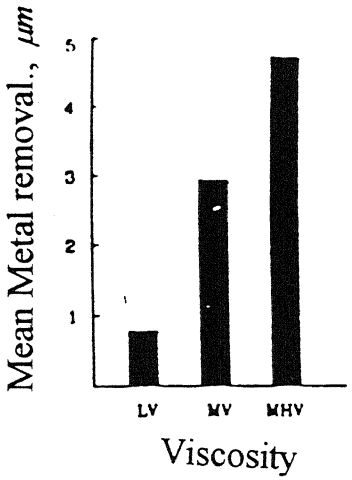

Fig 1.1 (a) Effect of media viscosity on material removal
[Williams R.E., Rajurkar K.P,1989]

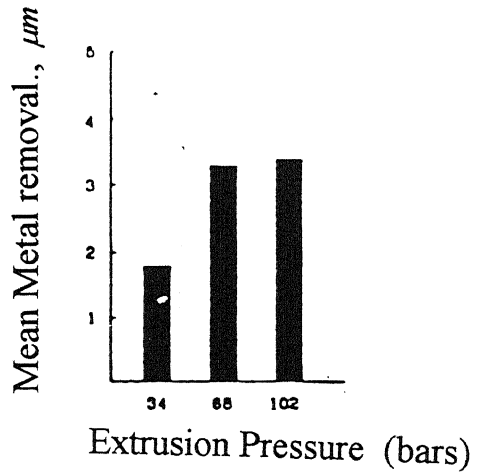

Fig 1.1 (b) Effect of pressure on material removal
[Williams R.E., Rajurkar K.P,1989]

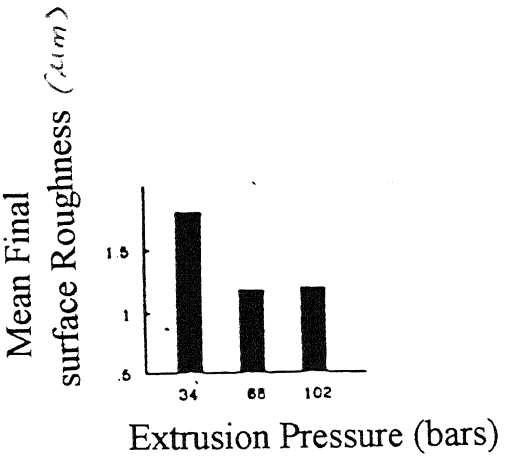

Fig 1.1 (c) Effect of pressure on suface roughness
[Williams R.E., Rajurkar K.P,1989]

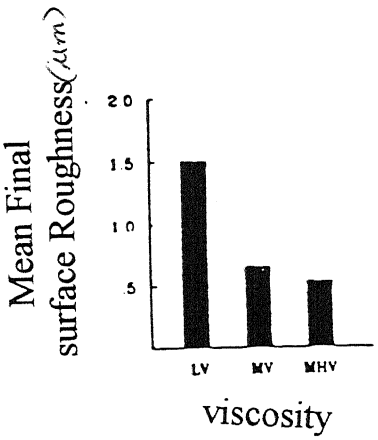

Fig. 1.1(d) Effect of media viscosity on surface roughness
[Williams R.E., Rajurkar K.P,1989]

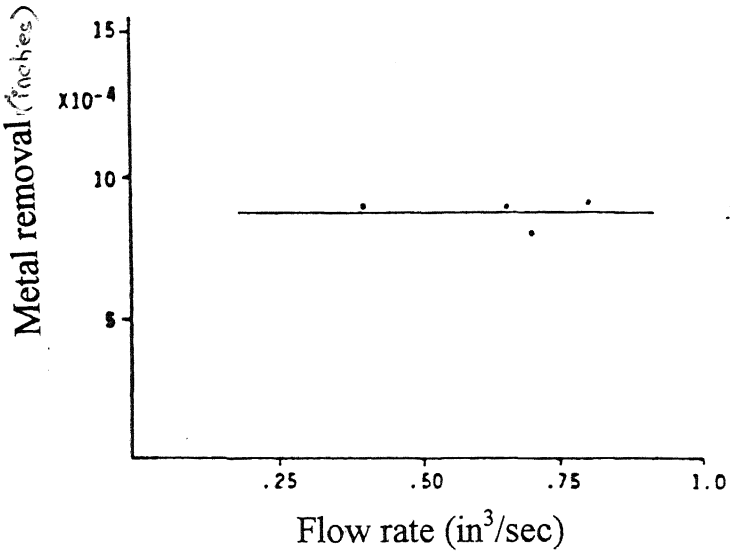

Fig 1.2 Effect of media flow rate on material removal

[Williams R.E., Rajurkar K.P, 1989.]

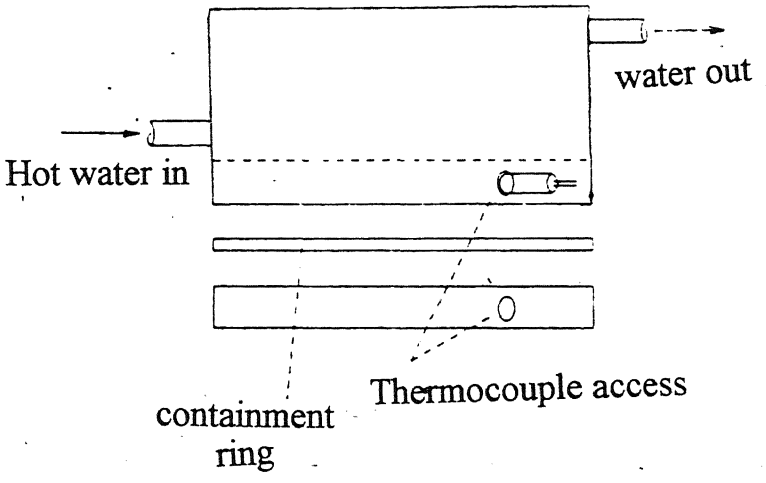

Fig 1.3 Modified Lees disc apparatus [Fletcher,1996]

a = steel cylinder
b = cavity for composite
c = heating element
d = thermocouple
e = cover plate
f = insulation layer

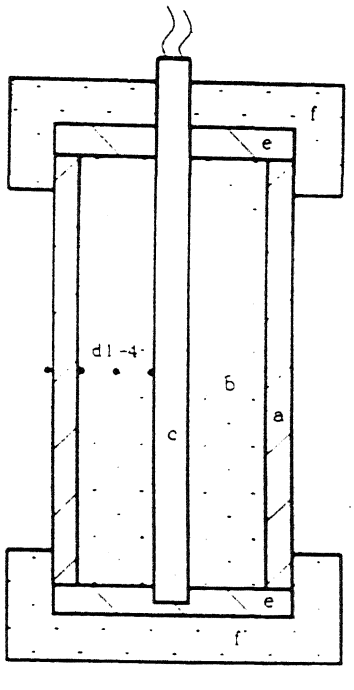

Fig.1.4 Surface heat transfer coefficient test apparatus (thermocouple positions included) [Fletcher,1996]

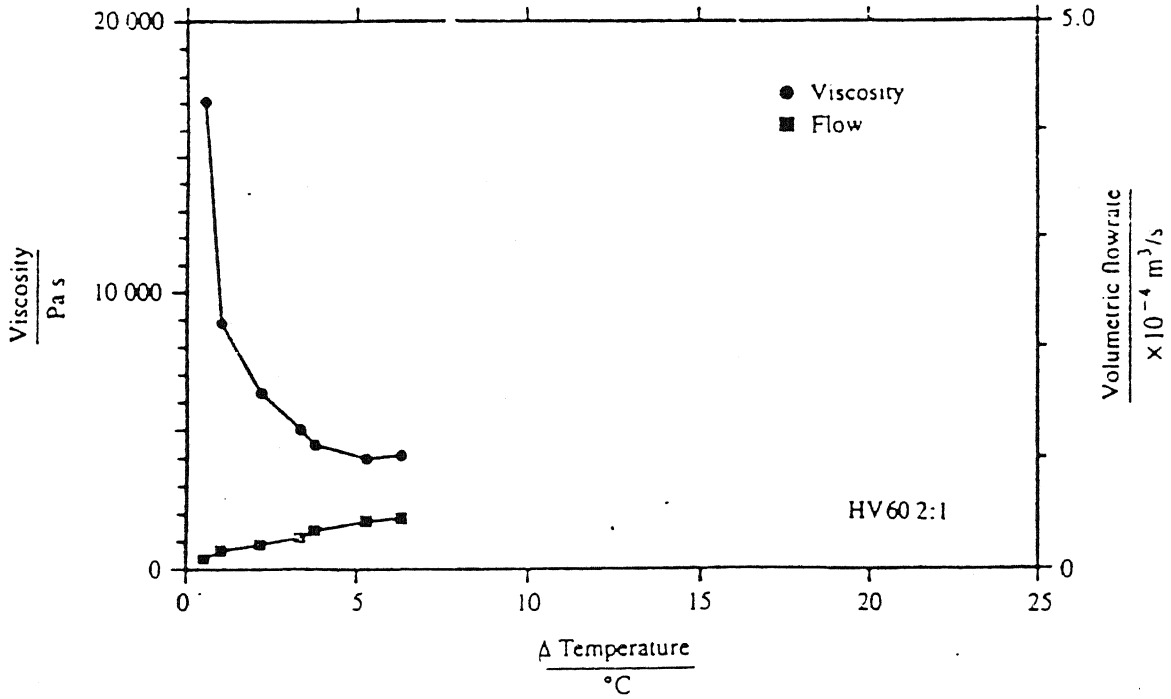

Fig 1.5. Relationship between change in temperature and the viscosity and volumetric flow rate of media [Davies,1996]

Chapter 2

VISCOMETRY

2.1 Non-Newtonian behaviour

In general, any fluid which doesn't show the linear relationship between the shear stress and shear rate is referred to as non-Newtonian fluid. Many complex non-Newtonian fluids are not purely viscous however, shear stress and shear rate ratio of these quantities is defined as rheological characteristic analogous to the Newtonian viscosity which is termed as *apparent viscosity* function. The fluids are classified by the way in which the shear stress varies with shear rate. Some of the most common classification of non-Newtonian behaviour as follows:

2.1.1 Plastic (Viscoplastic or Bingham Plastic)

This material behaves as an ideal rigid solid when subjected to shear stress smaller than certain yield value. For stresses above the yield value, the Bingham plastic behaves as a Newtonian fluid with shear stress being the linear function of shear rate. This behaviour is shown in Fig. 2.1(a). This type of behaviour is found in materials like pastes, suspensions, slurries, paints, putty etc.

2.1.2 Pseudoplastic (Shear thinning)

These materials exhibit a decrease in apparent viscosity as the shear rate increases. The apparent viscosity curve is qualitatively similar to that of the

Bingham plastic, Fig. 2.1(b). However, there is no actual yield stress, as the shear rate vs shear rate curve passes through the origin. In case of polymer and polymer solution, this curve rises rapidly and then flattens out at a relatively low shear rate.

2.1.3 Dilatant (Shear thickening)

These type of materials expand or dilate when subjected to shear stresses and also tend to exhibit an increase in apparent viscosity with the shear rate because of this dilation property, Fig 2.1(b). This type of behaviour is found more in some concentrated suspensions of solids, slurries, proteins and certain polymer solutions.

2.1.4 Structural Viscosity

This is more general type of shear thinning behaviour characterized by three different and distinct regions: a Newtonian region at low shear rates, a non-linear region at the intermediate shear rates, and another Newtonian region at high shear rates. The zero viscosity is greater than the high shear limiting value as shown in Fig. 2.1(B). The different regions were due to the basic change in structure of the material as a function of shear rate, hence the term is called as structural viscosity. This type of behaviour is found in macromolecules (particularly coiled polymers), many slurries and some lubricating oils. [Ronald Darby, 1976]

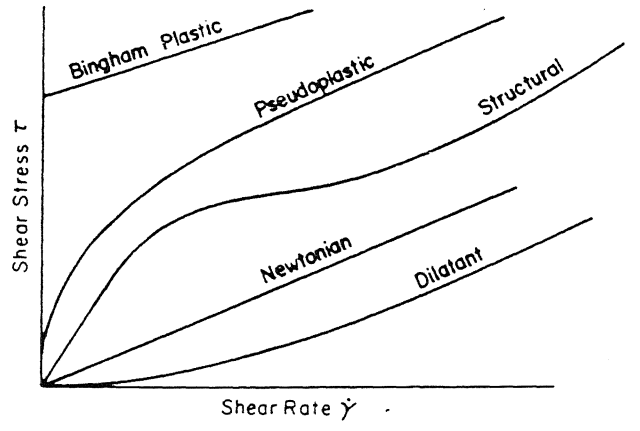

(a)

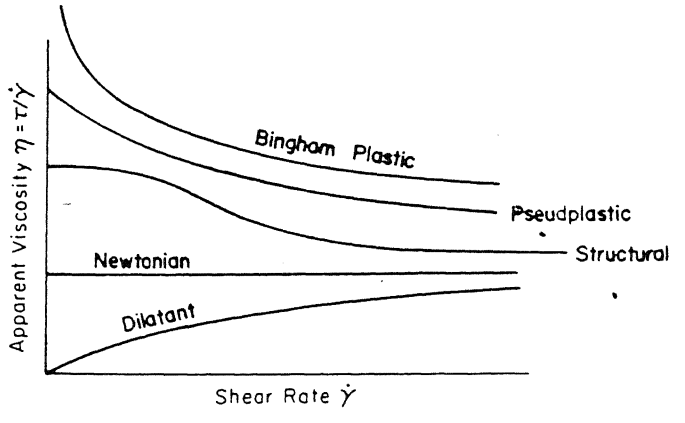

(b)

Fig 2.1 Classes of non-Newtonian behaviour [Ronald . Darby, 1976]

2.2 Capillary Viscometry

In order to determine the rheological property (apparent viscosity) of the non-Newtonian fluids, experimental methods have been developed. The viscometer developed based on the principle of capillary viscometry is the one used to experimentally determine the viscosity of the fluids in the present case. Hagan-Poiseuille studied capillary flow problems and derived relations between

the flow rate and pressure drop considering the steady axial flow of an incompressible fluid in a circular tube.[Van Wazer, 1963].

2.2.1 Mechanics of Capillary

In capillary viscometry, the media is forced through a fine-bore tube and the viscosity of the media is determined from the volumetric flow rate, applied pressure and tube dimensions.

The following assumptions have been made in capillary viscometry:

- The flow is steady.
- There are no tangential and radial components of velocity.
- There is no slippage at the wall (this condition postulates that axial velocity, $u = 0$ at $r = R$), where R is radius of the tube.
- The fluid is incompressible.
- There are no external forces.
- The tube is sufficiently long such that end effects are neglisibe.

Consider a fluid flowing in a circular tube as shown in Fig. 2.2 For the laminar steady flow, the viscous force tending to retard the flow will be exactly equal to the force resulting from the pressure difference between the two ends.

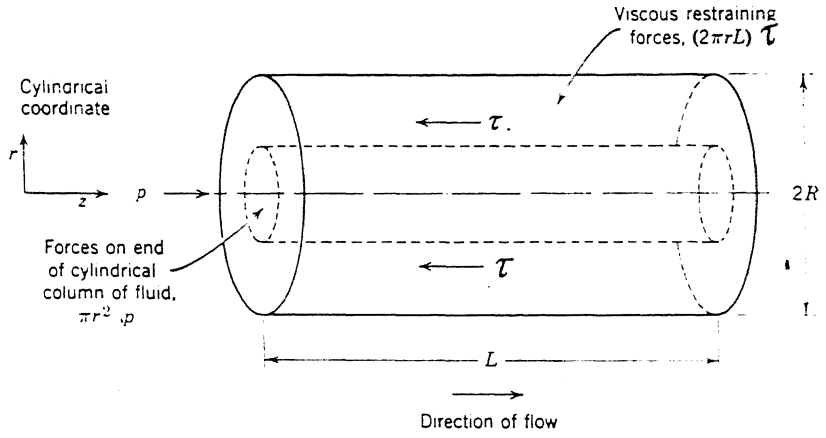

Fig. 2.2 Flow through a capillary [Van Wazer, 1963]

The viscous force F_v tending to prevent the cylindrical column from moving is

$$F_v = \tau . A = \tau . (2\pi rL) \qquad \text{.....(2.1)}$$

where, τ = shear stress in N/m^2

A = area of cross-section of the tube in m^2

L = length of the tube in m

The applied force tending to move the cylindrical column in the direction of the flow is equal to $p.(\pi r^2)$ .....(2.2)

where, p = Pressure drop across the capillary in N/m^2

For steady flow, these two forces must be equal

$$\tau(2\pi rL) = p.\pi r^2 \qquad \text{.....(2.3)}$$

From the equation 2.3 shear stress obtained as

$$\tau = \frac{pr}{2L} \qquad \text{.....(2.4)}$$

where, $\frac{p}{L}$ = pressure gradient across the capillary.

From the above equation (2.4), the shear stress in the fluid flowing through a capillary is directly proportional to the distance from the centre of the capillary and to the pressure gradient. The maximum shear stress occurs at the wall of the tube (where r = R)

The shear stress at the wall, $\tau_w = \frac{pR}{2L}$ .....(2.5)

2.2.2 Apparent viscosity

Apparent viscosity function of the fluid requires the determination of the shear rate. The rate of shear (γ) is always a function of shear stress for the given fluid.

$$\gamma = \frac{-du}{dr} = f(\tau) \qquad .....(2.6)$$

where, $\frac{-du}{dr}$ = shear rate in s^{-1}

u = axial velocity of the fluid in the tube in m/s.

The volumetric flow rate is written as $Q = \int_0^R 2\pi r u(r)\, dr$ .....(2.7)

On integration of the equation (2.7) by parts

$$Q = 2\pi u \int_0^R r dr - 2\pi \int_0^R \frac{du}{dr} dr \int r dr$$

$$Q = \left|\pi r^2 u\right|_0^R - \pi \int_0^R r^2 \frac{du}{dr} dr \qquad .....(2.8)$$

$$Q = -\pi \int_0^R r^2 \frac{du}{dr} dr \qquad .....(2.9)$$

Since u = 0 at r= R, $\frac{r}{R} = \frac{\tau}{\tau_w}$ and $\frac{-du}{dr} = f(\tau)$ transformation of variables in the above equation gives

$$Q = \frac{\pi R^3}{\tau_w^3} \int_0^{\tau_w} \tau^2 f(\tau)\, d\tau$$

$$\frac{4Q}{\pi R^3} = \frac{4}{\tau_w^3} \int_0^{\tau_w} \tau^2 f(\tau)\ d\tau \qquad (2.10)$$

In the above equation shear rate is expressed as the function of shear stress

Therefore, the apparent shear rate $\gamma = \frac{4Q}{\pi R^3}$ .....(2.11)

2.2.2.1 Empirical model for Bingham plastic materials

The Bingham plastic material behaves as a Newtonian fluid beyond the yield stress of the material. The general form of constitutive equations used for Bingham plastic materials which exhibit yield stress and shear rate are similar to that Newtonian-fluid as shown in equations 2.5 and 2.11.

$$\dot{\gamma} = 0, \quad \text{for} \quad \tau < \psi$$

$$\tau = \psi + \eta_{pl}\dot{\gamma} \quad \text{for} \quad \tau > \psi$$

where, ψ = yield stress of the material

The plastic viscosity (η_{pl}) is calculated as

$$\eta_{pl} = \frac{\tau_w - \frac{4}{3}\psi}{\frac{4Q}{\pi R^3}}$$

The apparent viscosity function is determined as, $\eta_a = \eta_{pl} + \frac{\psi}{\gamma}$

The yield stress ψ of the material is found out by plotting the graph between the apparent shear rate and wall shear stress. Using the method of least squares for fitting the data to a straight line and the yield stress of the material is determined by extrapolating the straight line onto the x-axis and the intercept made on the x-axis at zero shear rate gives the value of $\frac{4}{3}\psi$ (3/4th of this value gives the value of ψ)[Van Wazer]. The slope of the straight line gives the reciprocal of Plastic viscosity (η_{pl}) as shown in Fig. 2.3.

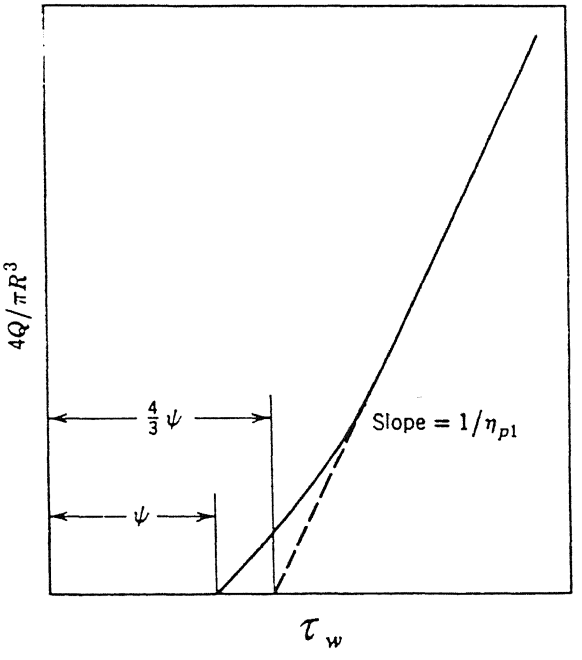

Fig. 2.3. Relationship between the wall shear stress and shear rate

Chapter 3

EXPERIMENTAL SET - UP AND EXPERIMENTATION

Experiments are conducted on the capillary viscometer designed for the measurement of viscosity. The present chapter deals with its details related to design and working of the set-up.

3.1 Viscometer set-up

Viscometer set-up has been designed using the principle of capillary viscometry. In this method, the media filled in the tube is forced through a fine-bore tube and the viscosity of the media is calculated by measuring its volumetric flow rate, applied pressure and tube dimensions. The drawing of the assembled set-up is shown in Fig 3.1(a) and photograph of setup in Fig 3.1b. The assembled set-up is fixed to the table.

The set-up consists of hollow cylinder (Fig 3.2) covered with covering plates both at the top and bottom and welded to the cylinder, to avoid leakage of water from the cylinder. Hollow cylinder (Fig 3.2) consists of inlet and outlet (Fig 3.3) at the top and bottom for the circulation of water inside the cylinder. The cylindrical tube selected is sufficiently long so that the end effects are neglisible. The tube is inserted through the holes made at the center of the cover plates (Fig 3.4), and it is welded at the bottom of the cover plate to prevent sliding of the tube inside the cylinder. Thermocouples (Chromel-Alumel) are fixed at the bottom of the cylindrical tube (Fig 3.5) with the help of

cylindrical cup. To measure the temperature of the media touching inside periphery of the tube surface, a hole of diameter 4.5mm on the cylindrical tube is made below the bottom cover plate. A semi-circular brass piece (Fig 3.6) having a hole of 6 mm with internal threading is aligned with the hole made on the cylindrical tube and is sealed to the tube surface with araldite. A perspex screw (Fig 3.7) having a hole of 2 mm (to insert thermocouple bead) is tightened in semi-circular brass piece. The screw is tightened in brass piece upto which thermocouple bead touches the media inside the tube. To measure the core temperature of the media cylindrical cup (Fig 3.8) having a hole of 6 mm diameter with internal threading at the bottom of the cup is attached to the bottom of the cylindrical tube. The thermocouple bead is inserted into the hole made in the perspex screw which is screwed at the bottom of the cylindrical cup. The cylinder is insulated by wounding asbestos rope (Fig 3.1). The temperature of the media is increased by constant circulation of heated water around the cylindrical tube. The temperature of the water is controlled by constant temperature bath (Fig 3.1). The temperature upto which water is to be heated, is controlled by adjusting the knob of contact thermometer (Fig 3.1). If the temperature set in contact thermometer is above the initial temperature of water then the heater starts heating the water in the bath. Once the temperature set in contact thermometer is achieved, the heater is automatically switched off. The heated water in the bath is circulated by pump in constant temperature bath, through the inlet of the cylinder. The outlet of the cylinder is connected to the inlet of the constant temperature bath. Water from the bath is continuously circulated into the cylinder until it reaches the desired temperature set by contact thermometer. The rise in temperature of the media at the inside periphery of the tube and at the core can be found out by measuring the voltage difference

of thermocouples. This voltage difference is converted into the temperature with the help of calibration graph for the given thermocouple.

3.2 Experimental Procedure

Abrasive media is filled into the tube upto its three-fourth length.. Before filling the media into the tube, it is closed at the bottom by cylindrical cup. The media is then compacted by placing the 20 kg weight on the rod-disc assembly (Fig 3.9) which acts as a piston to force the media inside the cylindrical tube, for about half an hour. This procedure is repeated until the tube is filled with the media upto three-fourth of its length. Before setting the temperature in the bath, fix the thermocouples at the inside periphery of the tube as well as at the core. The temperature of water is increased in the bath by contact thermometer. After setting temperature in the bath, put on the voltage recorder upto the time interval of 45 minutes. This time interval is kept constant in all the experiments, because the change in temperature of the media almost stabilizes within the time interval. Fig. 3.10 shows the temperature rise plotted by the recorder for concentration 60% and mesh size 100 and with 10^0C rise of water temperature. It can be observed from the Fig 3.10 that the temperature rise of the media is almost stabilizes after the time interval of 45 min. After measuring the rise in media temperature, now the pressure is applied on the media by placing weights on the rod-disc assembly (Fig 3.9). The tube is closed at the bottom by cylindrical cup. Then, length of the extruded material is measured for a time interval of five minutes. This procedure is repeated at different temperatures and pressures. Table 3.1 and 3.2 shows the conditions under which the experiments have been conducted.

Table 3.1 Experiments conducted at room temperature

S.No.	% conc.	Mesh size	weight applied w (kg)
1	50, 60, 70	100 150 180	23.7, 28.7, 33.7, 38.7
2	80	100 150 180 240	23.7, 28.7, 33.7, 38.7

Table 3.2 Experiments conducted at different temperatures

Increase in water Temperature (^{0}C)	% conc.	Mesh size	weight applied w (kg)
10, 20, 30	50 60 70	100	23.7, 33.7, 43.7, 53.7
10, 20, 30	70	100 150 180 240	23.7, 33.7, 43.7, 53.7

3.3 Assembly and Part drawings

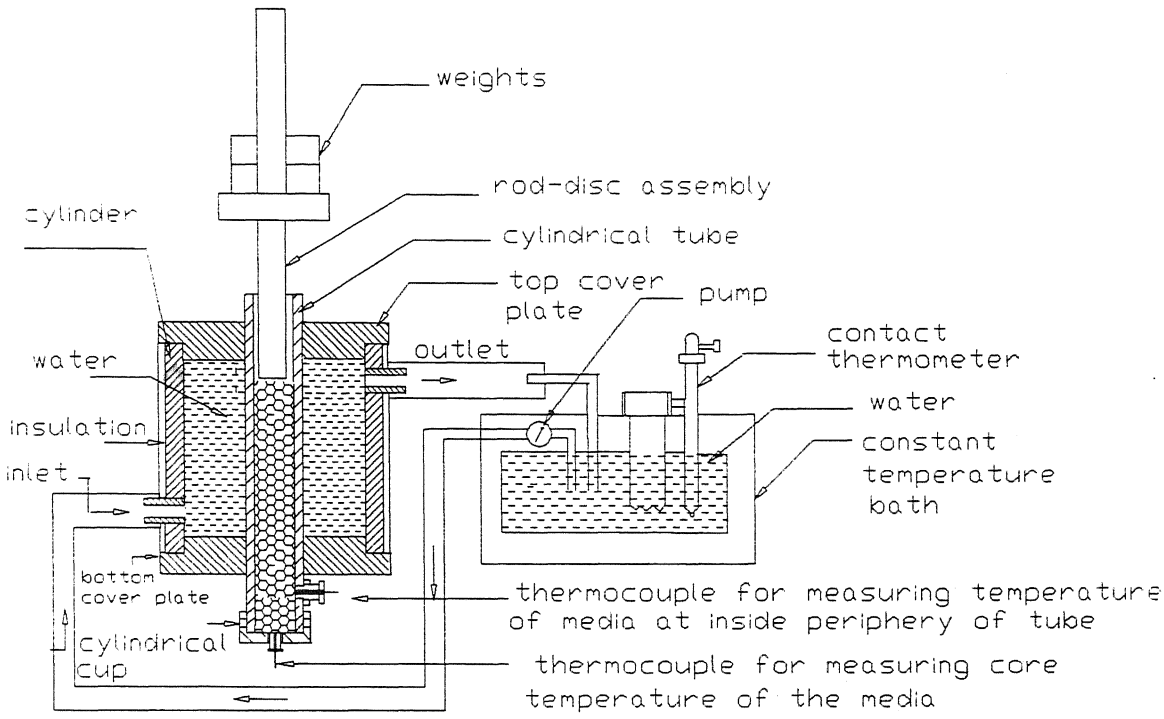

* Note : Not to the scale

Fig 3.1(a) Assembly drawing of Capillary Viscometer set-up

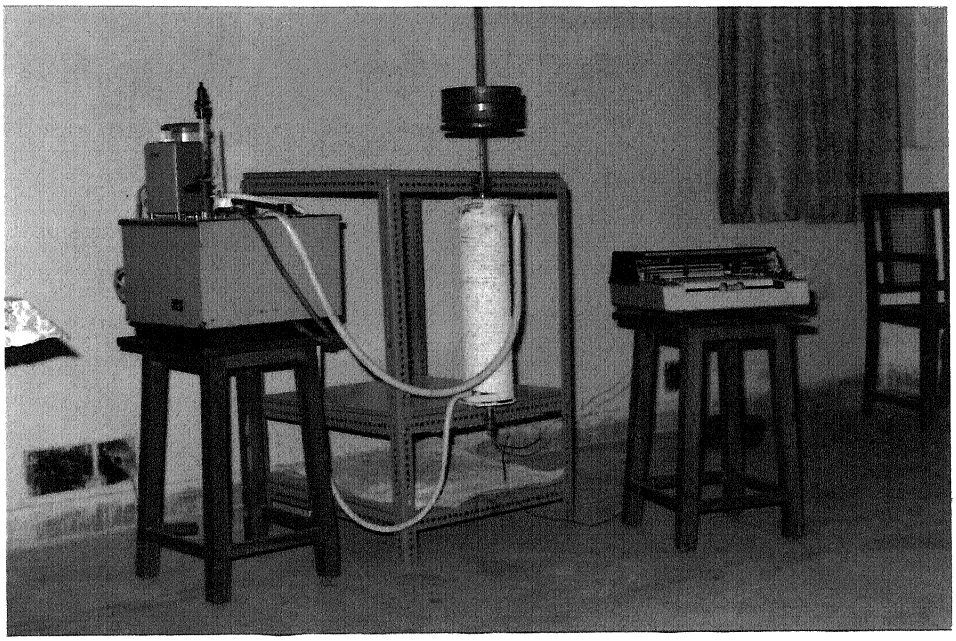

Fig 3.1(b) Photograph of the Experimental Set-up

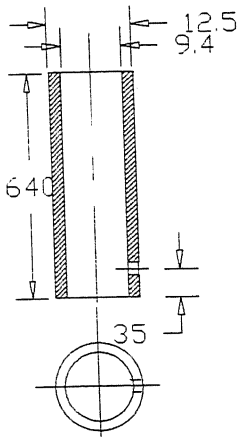

Fig 3.2 Hollow cylinder

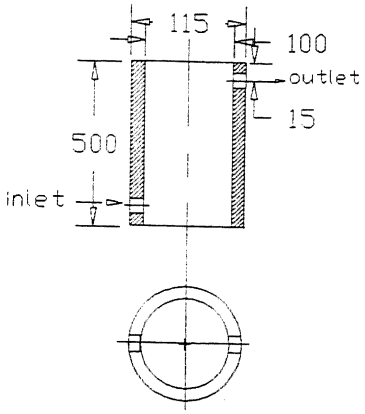

Fig 3.3 Inlet & outlet

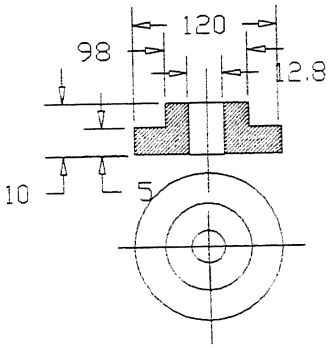

Fig 3.4 Cover plate

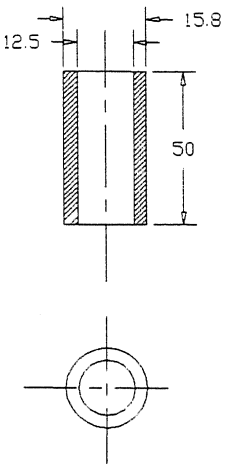

Fig 3.5 Cylindrical tube

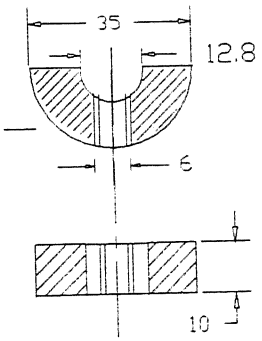

Fig 3.6 Semi-circular brass piece

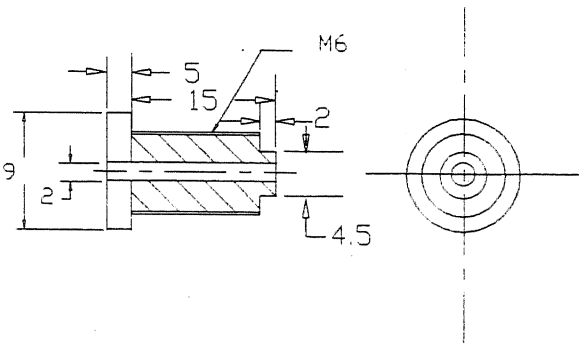

Fig 3.7. Perspex screw

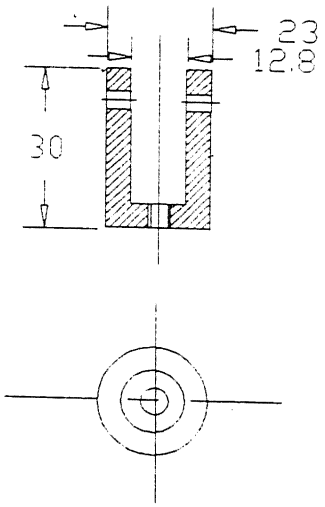

Fig 3.8 Cylindrical cup

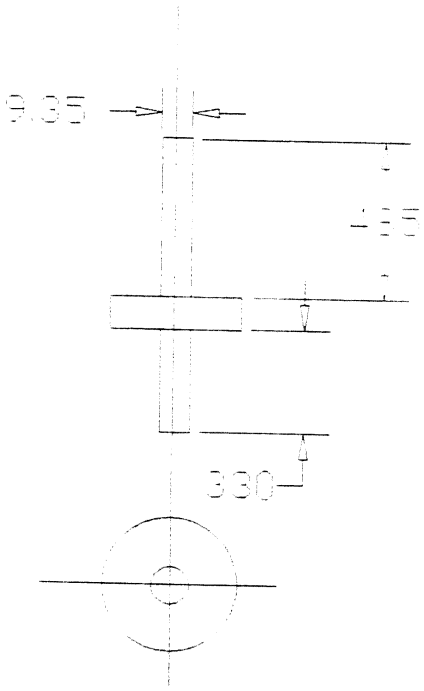

Fig 3.9 Rod-disc assembly

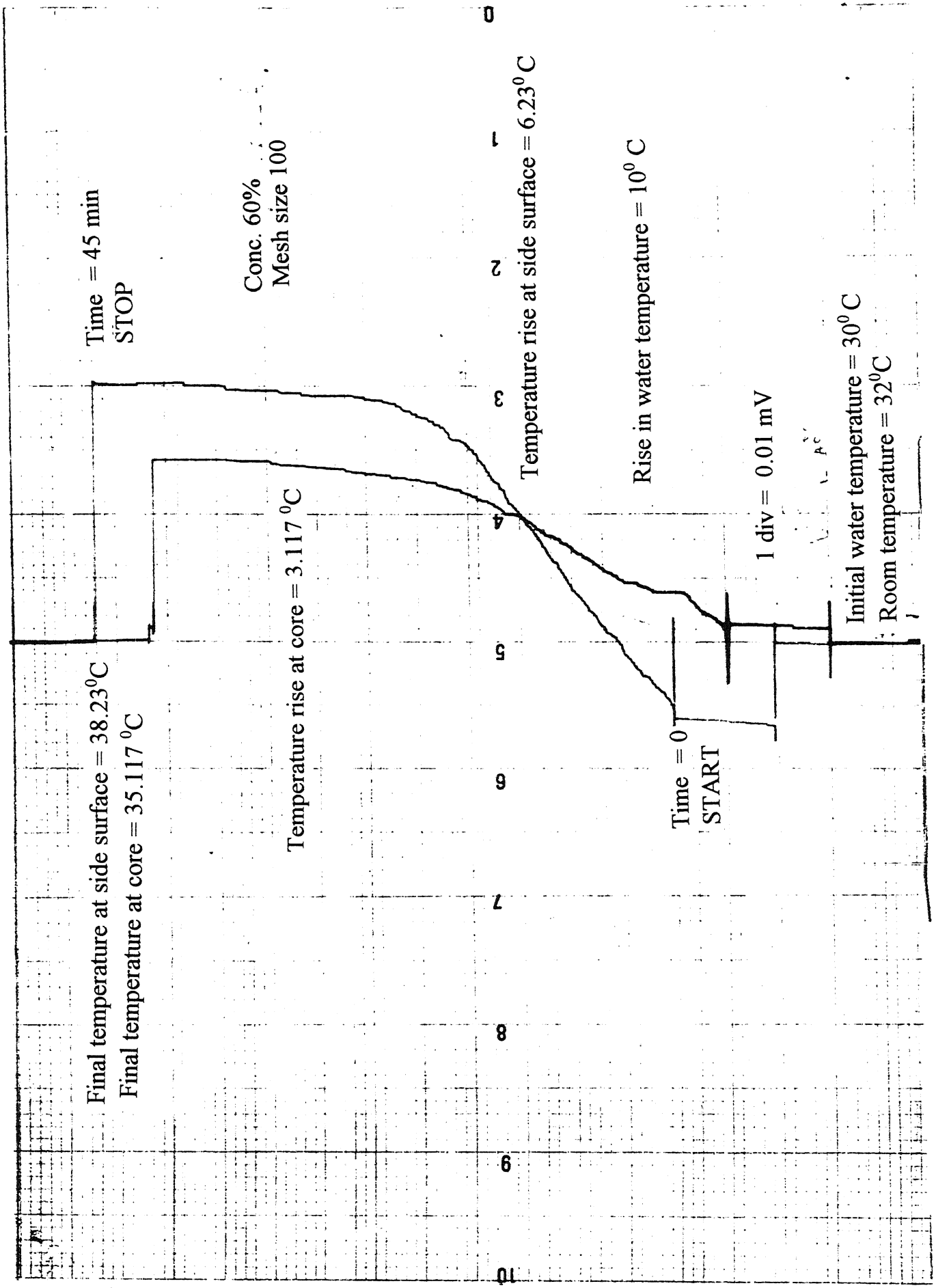

Fig 3.10 Rise in temperature plotted by recorder

The experimentation procedure discussed above involves following steps to determine the viscosity of the abrasive media.

1. Media preparation
2. Compaction
3. Heating
4. Measurement of temperature
5. Extrusion
6. Calculation of viscosity

3.4 Media preparation:

Media is a mixture of putty, silicon carbide abrasive particles and varnish oil. The size of the particles are shown in the table 3.2. To prepare the mixture in definite proportion to achieve the desired concentration. First 100 gms of pure putty is mixed with 15ml of varnish oil. Then the abrasive particles are mixed with the mixture of oil and putty on a glass plate to achieve the desired concentration. (% conc. by weight = $\frac{Abrasiveweight}{puttyweight}$ x 100). Before actually filling the media in the cylindrical tube, the media is mixed for 80 cycles with round wooden piece, so as to get the uniform mixture of varnish oil, abrasives and putty.

Table 3.3 : Abrasive particle sizes corresponding to mesh size[Malkin, 1989]

Size of abrasive particle $d_g = \frac{0.6x25.4}{m}$ mm, where m = mesh size

Mesh size	d_g (mm)
100	0.1524
150	0.1016
180	0.0847
240	0.0635

3.5. Compaction

The cylindrical tube in (Fig 3.5)is cleaned by turpentine oil before filling the media in it. The tube must be kept closed by cylindrical cup Fig (3.8) at the bottom of the cylindrical tube, and then the abrasive media is filled into the tube. The media is then compacted by placing the weight of 20kg on rod-disc assembly (Fig 3.9) for about half an hour. Compaction procedure is repeated until the tube gets filled upto three-fourth of its length.

3.6 Heating

The abrasive media filled in the tube is heated by constant circulation of heated water from the constant temperature bath to the cylinder. Before setting the temperature of water in the bath, note down the room temperature and initial water temperature by thermometer (measuring accuracy upto 0.5^0C). Before increasing the temperature of water, fix the thermocouples at the core and inside periphery of the tube surface, to measure temperature of the media. Increase the water temperature by 10^0C from its initial temperature by contact thermometer. If the temperature of the water set by contact thermometer is above its initial temperature, heater in the bath starts heating the water and it is continued until it reaches the desired temperature set by contact thermometer. The temperature achieved by the media in the tube is less than the temperature of water set by contact thermometer, because of decrease in temperature gradient during the constant circulation of heated water inside the cylinder. In actual AFM, also the system doesn't get enough time to have the same temperature of the whole media. It should be more like an average temperature because the mixing of the media takes place in different cycles.

3.7 Measurement of the temperature

The rise in temperature of the media is calculated by measuring the voltage difference across the thermocouples by recorder. The recorder is capable of measuring upto 0.005 mV. The recorder is calibrated with the rise in water temperature at different temperature rise of water. The voltage difference across the thermocouples is measured at known temperatures of water.

Table 3. 4 Calibrated Values

Temperature rise of water ΔT (^{0}C)	Voltage difference Δv (mV)
0	0.0
3	0.18
9	0.44
13	0.65
17	0.80
23	1.05
27	1.15

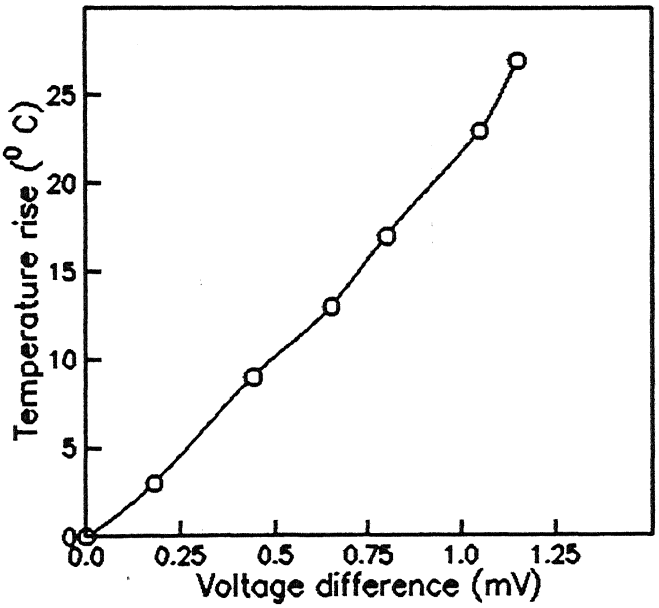

Fig 3.11 Calibration curve

The temperature rise is calculated from the equation obtained from the slope of the straight line shown in Fig 3.11

$$\Delta v = 0.0417 \Delta T$$

where, Δv = Voltage difference in mV.

ΔT = Temperature rise in ^{0}C.

The recorder is put on immediately after setting the rise in water temperature in the bath by contact thermometer. The rise in media temperature is plotted by the recorder for constant time interval of 45 min. The rise in temperature of media is calculated from the voltage difference of thermocouples plotted by the recorder.

3.8 Extrusion

After measuring the rise in temperature of the media, place the weights on the rod-disc assembly with tube closed at the bottom by cylindrical cup. Remove the cup (Fig 3.8) at the bottom of the tube after placing the weights on the rod-disc assembly (Fig 3.9) and extrusion is allowed to continue for the time interval of five minutes. The time interval is measured by a stop-watch. The length of the extruded material is measured by shearing off the extruded portion of the media with the help of a steel rule having accuracy of 0.5mm. Extruded media is again filled in the tube and compacted for 10-15 min and the same procedure is repeated at different pressures and temperatures.

3.9 Calculation of viscosity

The shear stress at the wall is calculated by the following equation

$$\tau_w = \frac{pR}{2L} \qquad \text{.....(2.5)}$$

where, $\frac{p}{L}$ = Pressure gradient across the length of the tube

R = Radius of the tube = 4.7 mm.

Pressure applied on the media = $\frac{w}{\pi r^2}$ ...(3.1)

where, w = weight applied on the media which includes weight of rod-disc assembly (3.7 kg).

r = radius of the piston on rod-disc assembly = 4.675 mm

As extrusion starts, the pressure gradient changes across the length of the tube, because the length of the media filled in the tube initially, does not remain constant as soon as the load is applied.

Assuming linear variation of 'L' with time as $L(t) = 0.48 - bt$ . ..... (3.2)

where, L(t) = length of media in the tube after the time interval 't',

b = constant

t = time interval ('t' = 5 min.).

The extruded length of the media is subtracted from the length of the media filled before the start of the experiment (i.e. 3/4 length of the tube which is equal to 480 mm), become the value L after 5 min and it is substituted in eq.(3.2) to calculate 'b' value. This 'b' value is evaluated for each experiment.

As 'L' varies with time, L(t) is integrated over the interval 0 to 5 min.

So, the actual value of $L = \frac{1}{5}\int_0^5 (0.48 - bt)dt$ .....(3.3)

This actual value of 'L' is used in the calculation of wall shear stress shown in eq.(2.5)

Apparent shear rate calculated as

$$\dot{\gamma} = \frac{4Q}{\pi R^3} \qquad .....(2.11)$$

where, Q = volumetric flow rate = $\frac{\pi D^2}{4}$ x u

D = inside diameter of the tube

Average extrusion velocity, u = $\frac{\text{extruded length}}{\text{time interval}}$

The Plastic viscosity, η_{pl} is calculated by

$$\eta_{pl} = \frac{\tau_w - \frac{4}{3}\psi}{\frac{4\dot{Q}}{\pi R^3}}$$

The apparent viscosity, η_a is calculated as

$$\eta_a = \eta_{pl} + \frac{\psi}{\dot{\gamma}}$$

where, ψ has been estimated as discussed in section 2.2.1.1

Experiments conducted under various conditions and the calculated results are given in Appendix - I.

Chapter 4

RESULTS AND DISCUSSION

4.1 Introduction

During the course of study, the media viscosity which has significant effect on material removal rate and surface finish in Abrasive flow machining (AFM) process is determined empirically from the calculations used for capillary viscometry. In this chapter, the results of viscosity at different concentrations and mesh sizes and temperatures are reported. And also, its effects on the process performance parameters such as material removal rate and surface finish are discussed.

4.2 Apparent Viscosity

The apparent viscosity is defined by the relation between the shear stress and shear rate (eq. 2.13). The first part of this section deals with the effect of wall shear stress on shear rate. The second and third part of this section deals with the effect of viscosity on wall shear stress and shear rate on the viscosity.

4.2.1 Effect of wall shear stress on shear rate

Fig 4.1(a-d) and Fig 4.2(a-f) show the effects of wall shear stress on the shear rate at different concentrations at room temperature as well as at different media temperatures. It is observed from the graphs that at different concentrations increase in the shear stress at the wall causes increase in the shear rate. As the shear stress at the wall causes increase in the extrusion velocity of the media which causes the increase in flow rate and thereby increase in the shear rate.

(a)

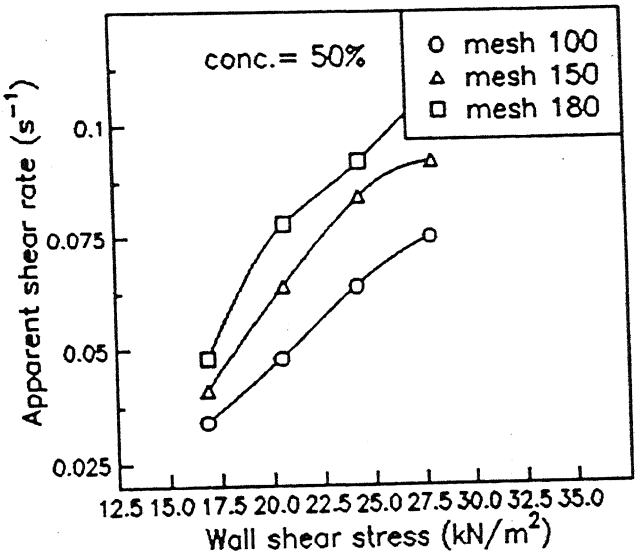
conc.= 50%
mesh 100
mesh 150
mesh 180
Apparent shear rate (s^{-1})
0.1
0.075
0.05
0.025
12.5 15.0 17.5 20.0 22.5 25.0 27.5 30.0 32.5 35.0
Wall shear stress (kN/m^2)

(b)

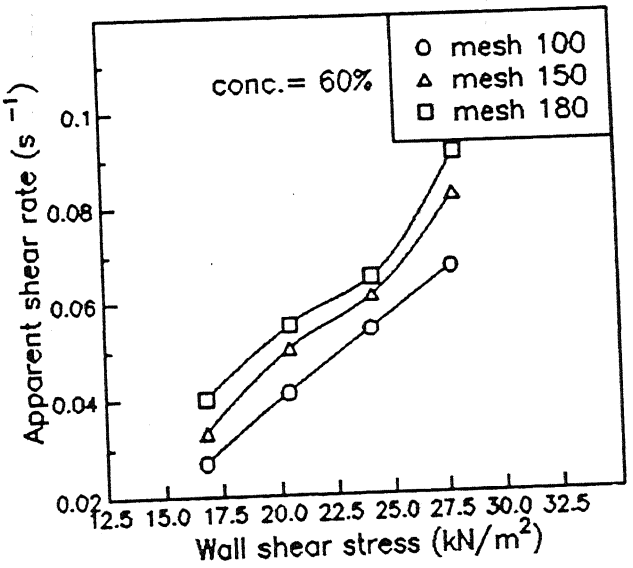
conc.= 60%
mesh 100
mesh 150
mesh 180
Apparent shear rate (s^{-1})
0.1
0.08
0.06
0.04
0.02
12.5 15.0 17.5 20.0 22.5 25.0 27.5 30.0 32.5
Wall shear stress (kN/m^2)

(c)

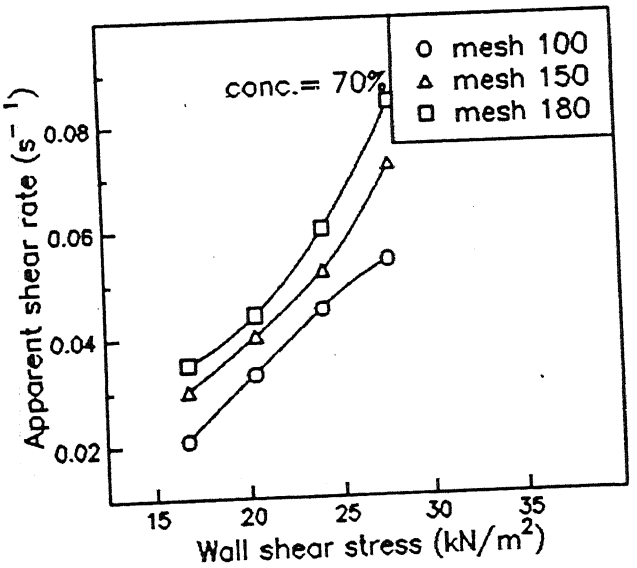
conc.= 70%
mesh 100
mesh 150
mesh 180
Apparent shear rate (s^{-1})
0.08
0.06
0.04
0.02
15 20 25 30 35
Wall shear stress (kN/m^2)

(d)

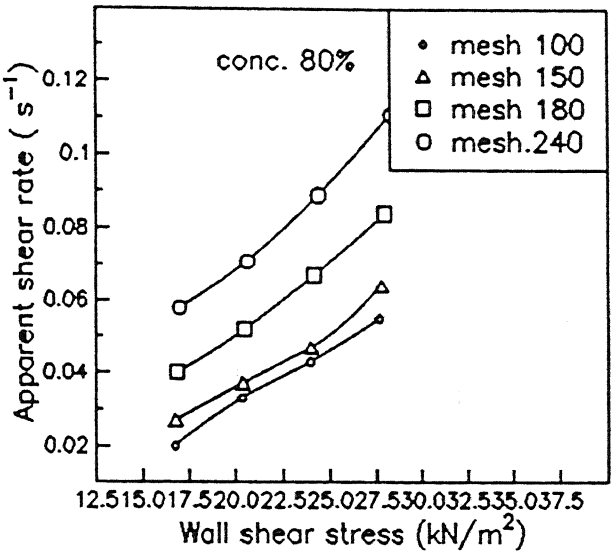

Fig.4.1 Wall shear stress v/s Apparent shear rate at different concentrations at room temperature

(a)

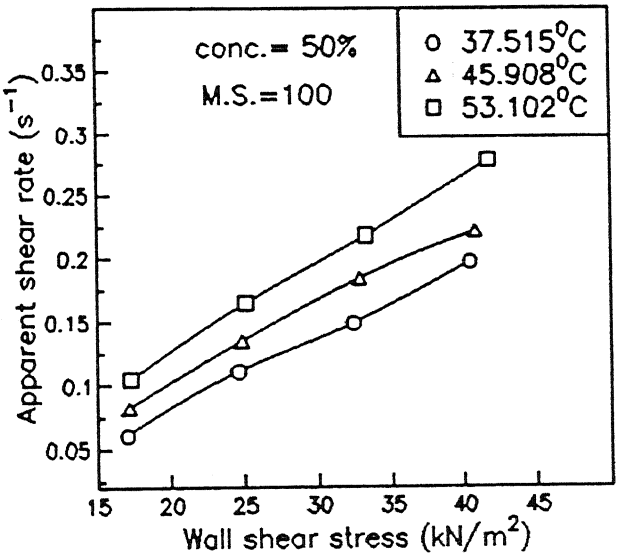

(b)

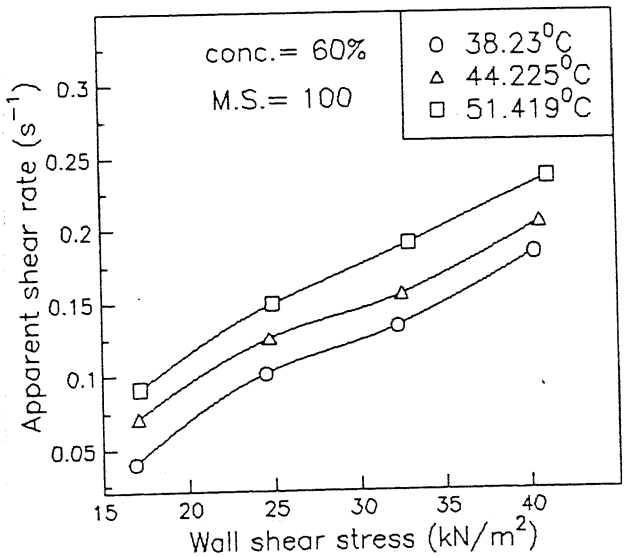

(c)

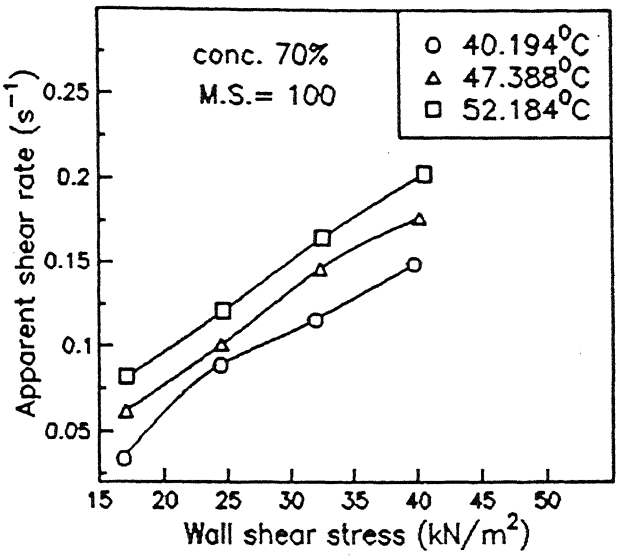
conc. 70%
M.S.= 100
40.194°C
47.388°C
52.184°C
Apparent shear rate (s⁻¹)
0.25
0.2
0.15
0.1
0.05
15 20 25 30 35 40 45 50
Wall shear stress (kN/m²)

(d)

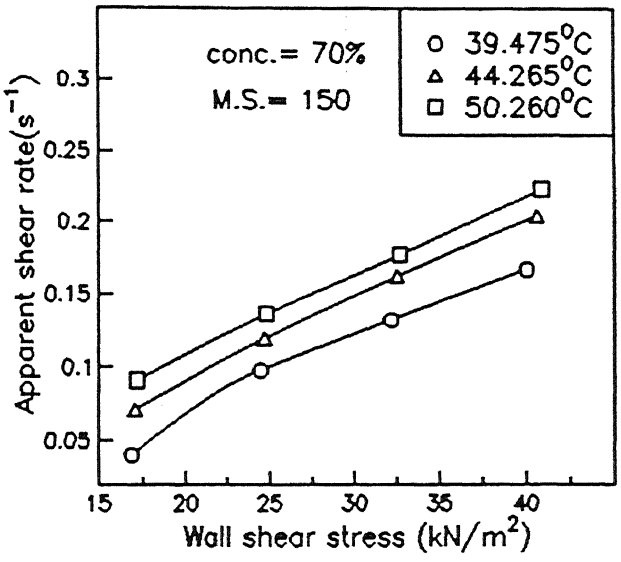
conc.= 70%
M.S.= 150
39.475°C
44.265°C
50.260°C
Apparent shear rate(s⁻¹)
0.3
0.25
0.2
0.15
0.1
0.05
15 20 25 30 35 40
Wall shear stress (kN/m²)

(e)

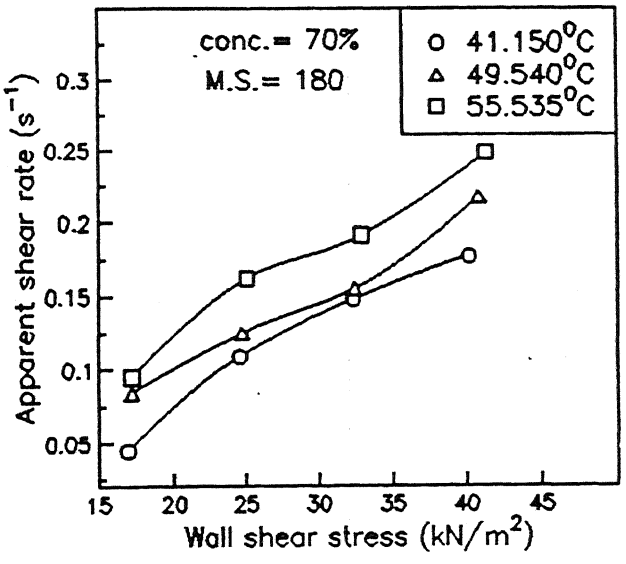
conc.= 70%
M.S.= 180
41.150°C
49.540°C
55.535°C
Apparent shear rate (s⁻¹)
0.3
0.25
0.2
0.15
0.1
0.05
15 20 25 30 35 40 45
Wall shear stress (kN/m²)

(f)

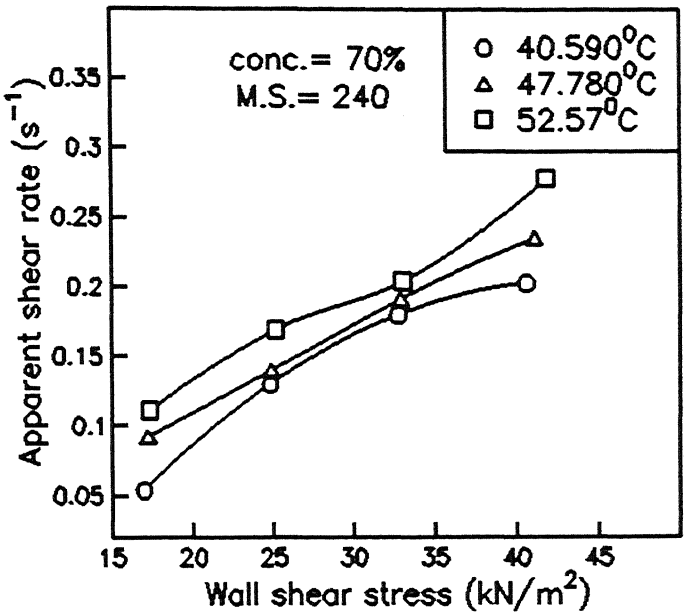

Fig. 4.2 Wall shear stress v/s Apparent shear rate at different media temperatures

4.2.2 Effect of Wall shear stress on Viscosity

Fig.4.3(a-d) shows that the effect of the wall shear stress on viscosity and at different abrasive sizes and concentrations. Fig.4.3(a-f) show the effect of wall shear stress on viscosity at different media temperatures and concentrations. It is observed from the graph that as the wall shear stress increases, there is a decrease in the apparent viscosity. This is due to the fact that increase in the wall shear stress increases the shear rate which means that it offers less resistance to the flow of the media thereby it decreases the viscosity of material.

(a)

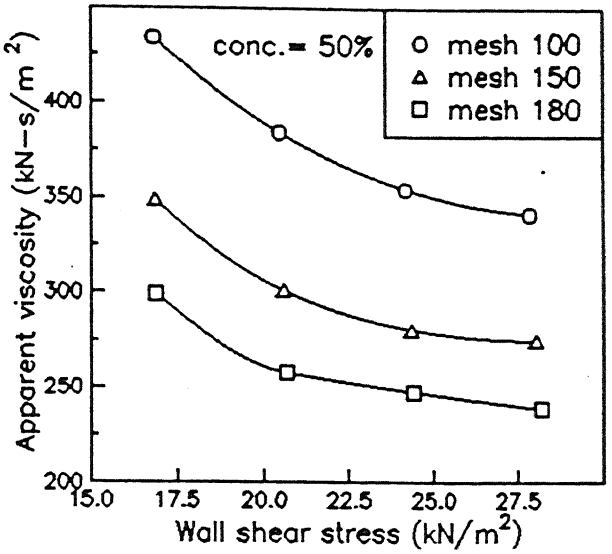
conc.= 50%
mesh 100
mesh 150
mesh 180
Apparent viscosity (kN-s/m 2)
400
350
300
250
200
15.0
17.5
20.0
22.5
25.0
27.5
Wall shear stress (kN/m2)

(b)

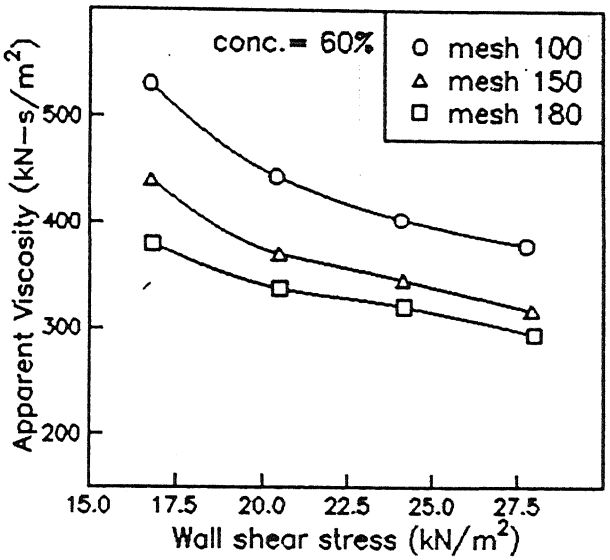
conc.= 60%
mesh 100
mesh 150
mesh 180
Apparent Viscosity (kN-s/m2)
500
400
300
200
15.0
17.5
20.0
22.5
25.0
27.5
Wall shear stress (kN/m2)

(c)

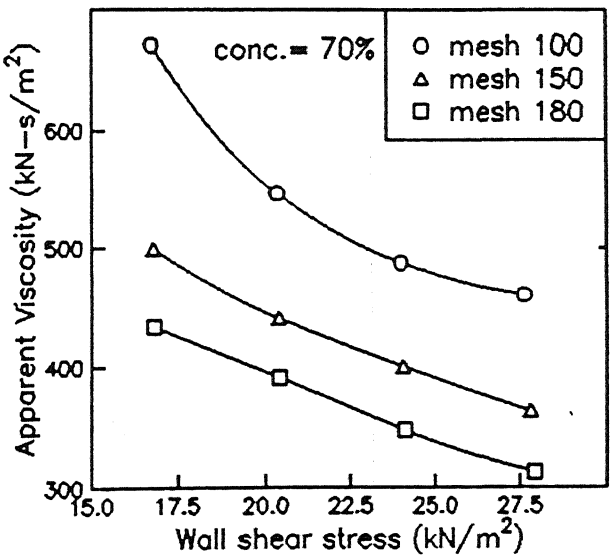
conc.= 70%
mesh 100
mesh 150
mesh 180
Apparent Viscosity (kN-s/m2)
600
500
400
300
15.0
17.5
20.0
22.5
25.0
27.5
Wall shear stress (kN/m2)

(d)

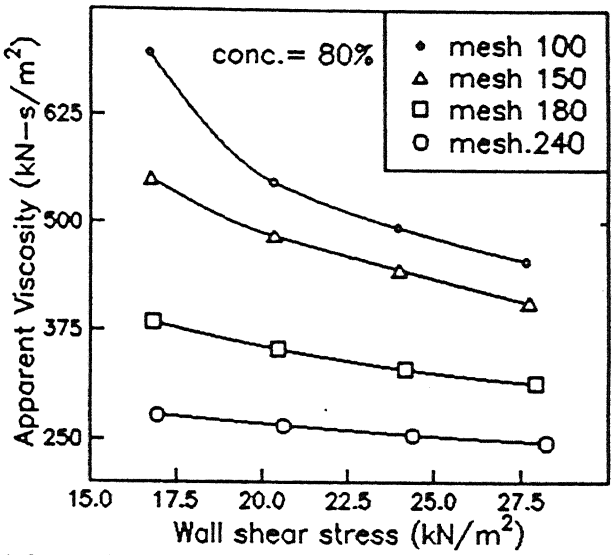

Fig.4.3 Wall shear stress v/s Apparent viscosity at different concentrations at room temperature

(a)

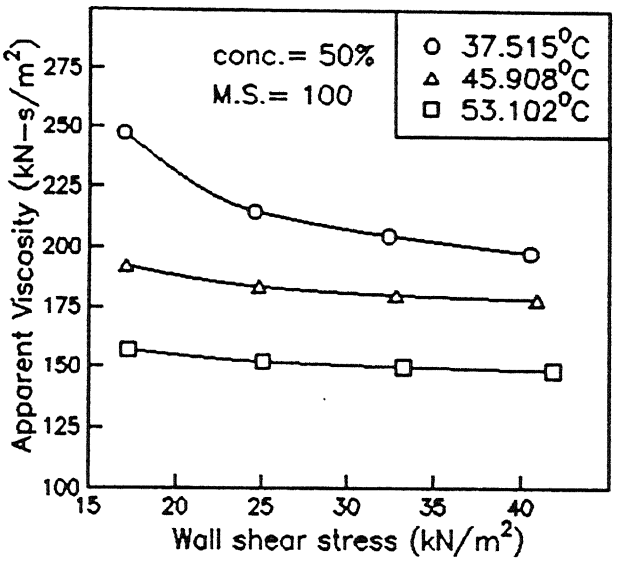

(b)

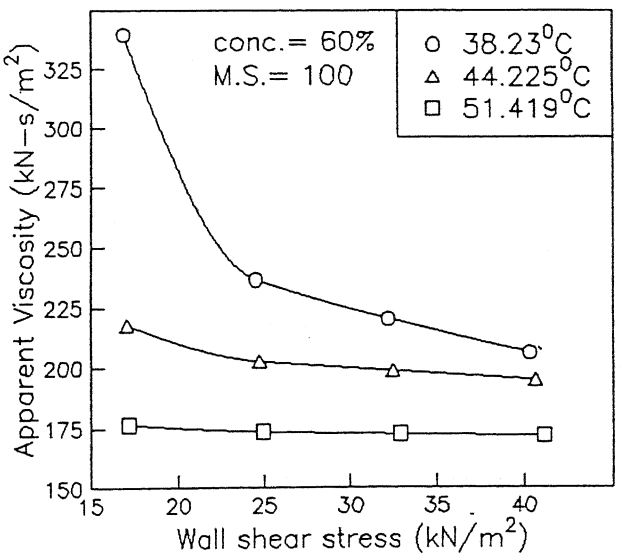

(c)

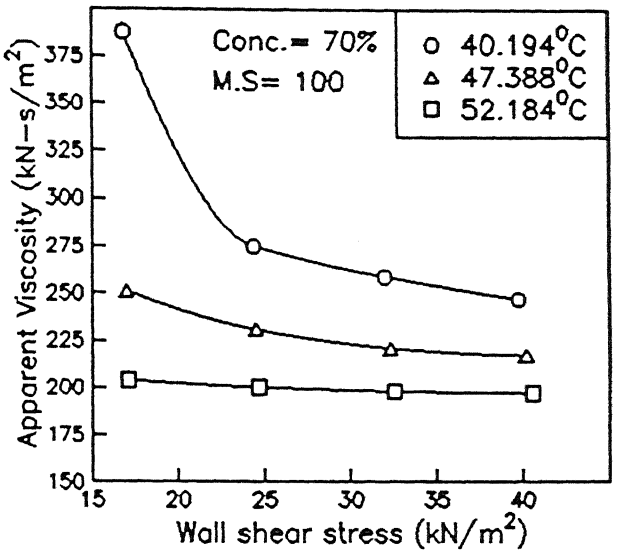
Conc.= 70%
M.S= 100
40.194°C
47.388°C
52.184°C
Apparent Viscosity (kN-s/m²)
375
350
325
300
275
250
225
200
175
150
15
20
25
30
35
40
Wall shear stress (kN/m²)

(d)

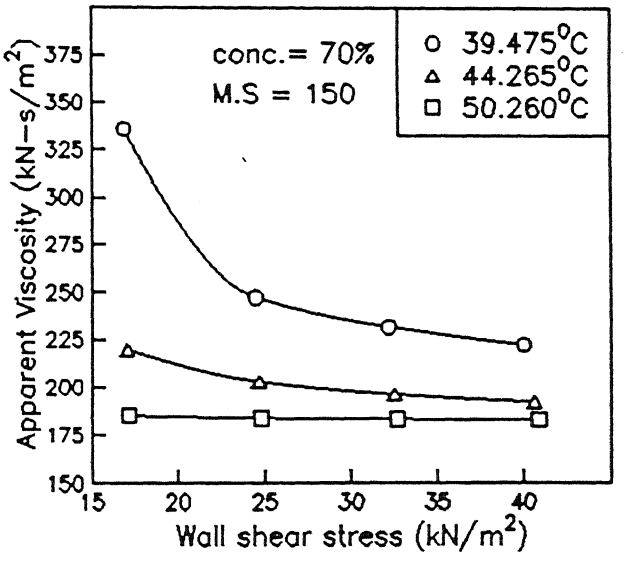
conc.= 70%
M.S = 150
39.475°C
44.265°C
50.260°C
Apparent Viscosity (kN-s/m²)
375
350
325
300
275
250
225
200
175
150
15
20
25
30
35
40
Wall shear stress (kN/m²)

(e)

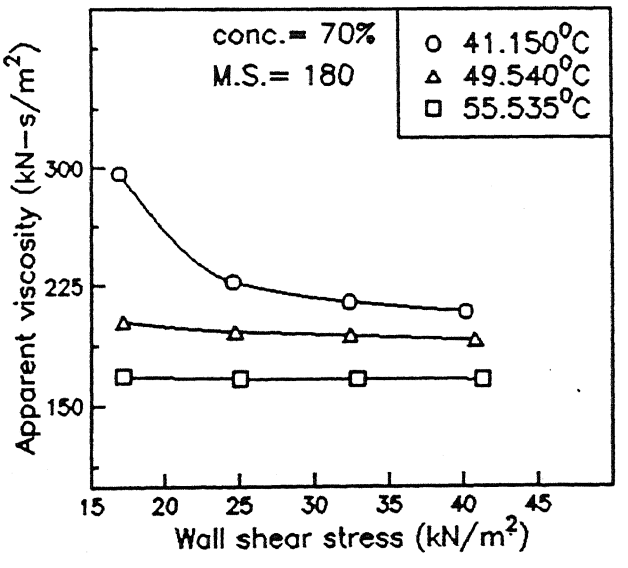
conc.= 70%
M.S.= 180
41.150°C
49.540°C
55.535°C
Apparent viscosity (kN-s/m²)
300
225
150
15
20
25
30
35
40
45
Wall shear stress (kN/m²)

(f)

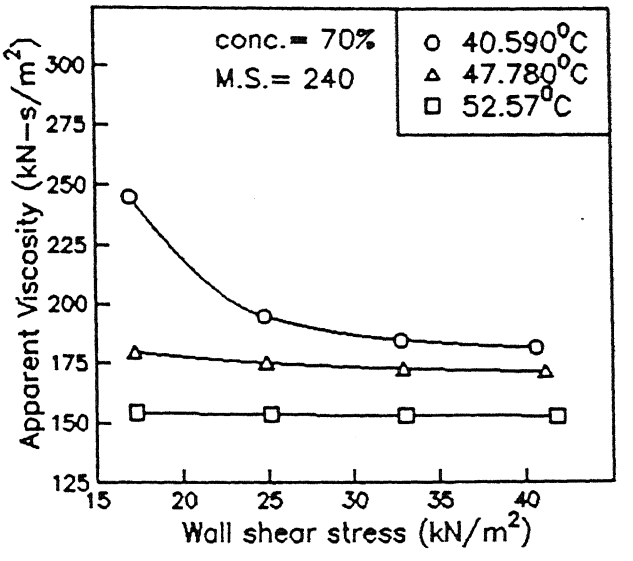

Fig 4.4 Wall shear stress v/s Apparent viscosity at different media temperatures

4.2.3 Effect of shear rate on viscosity

Fig.4.5(a-d) show the effect of shear rate on apparent viscosity shown at different abrasive concentrations and mesh sizes. Fig. 4.6(a-f) show the effect of shear rate on viscosity at different media temperatures for various concentrations. As the shear rate of the material increases, there is a decrease in the apparent viscosity of material. This type of behaviour is found in case of material which exhibit yield stress called Bingham plastic materials shown in Fig 2.1. This is due to the fact that as the shear rate increases causes increase in flow rate of the media which decreases in apparent viscosity of the material.

(a)

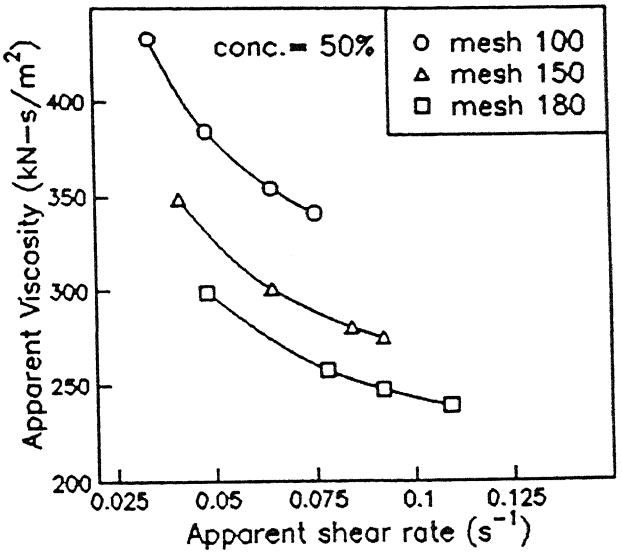
conc.= 50%
mesh 100
mesh 150
mesh 180
Apparent Viscosity (kN-s/m²)
200
250
300
350
400
0.025
0.05
0.075
0.1
0.125
Apparent shear rate (s⁻¹)

(b)

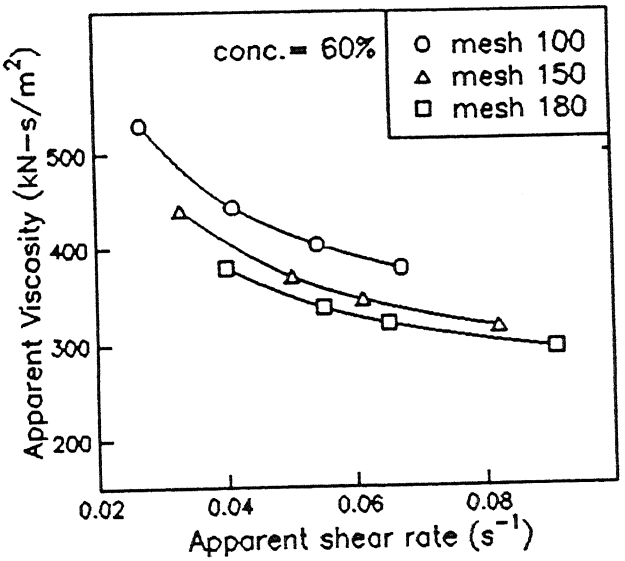
conc.= 60%
mesh 100
mesh 150
mesh 180
Apparent Viscosity (kN-s/m²)
200
300
400
500
0.02
0.04
0.06
0.08
Apparent shear rate (s⁻¹)

(c)

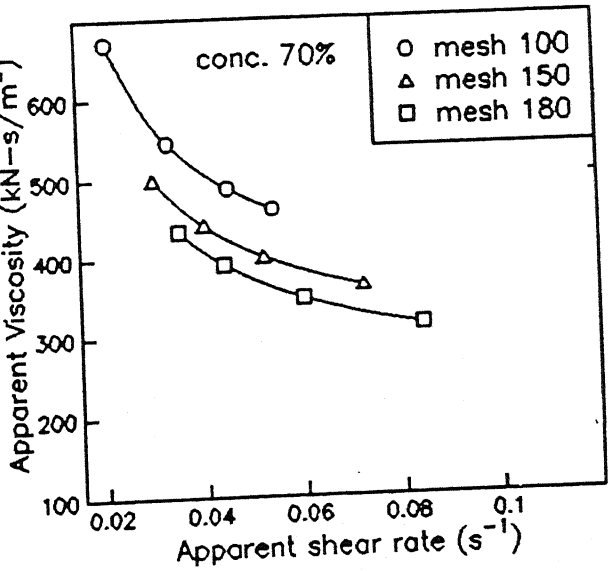
conc. 70%
mesh 100
mesh 150
mesh 180
Apparent Viscosity (kN-s/m²)
100
200
300
400
500
600
0.02
0.04
0.06
0.08
0.1
Apparent shear rate (s⁻¹)

(d)

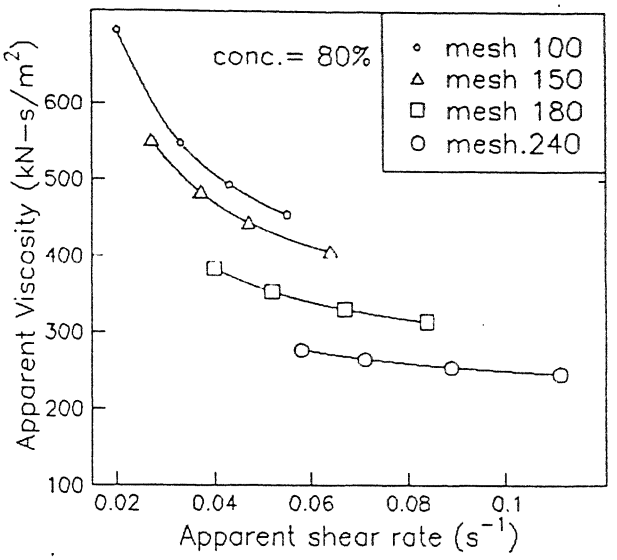

Fig. 4.5 Apparent shear rate v/s Apparent viscosity at different concentrations

(a)

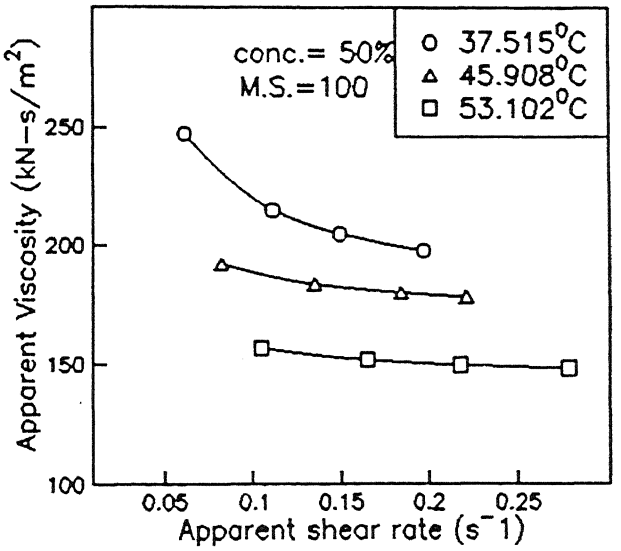

(b)

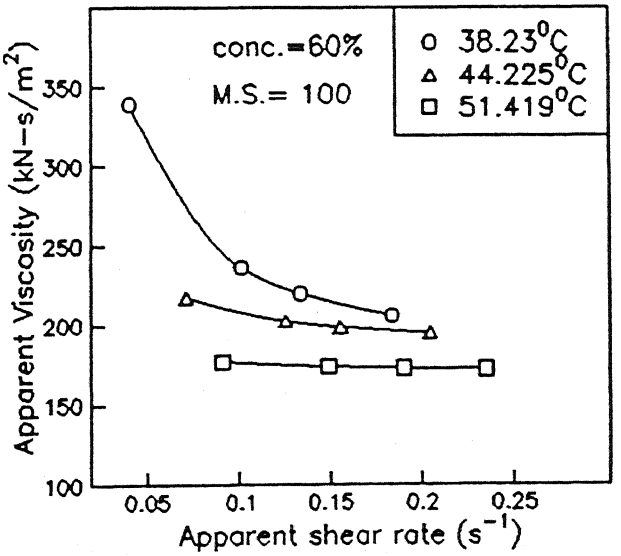

(c)

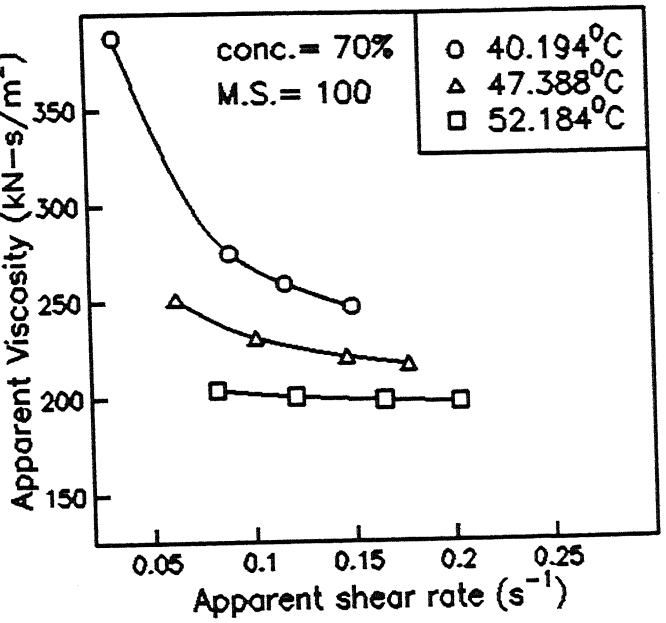
conc.= 70%
M.S.= 100
o 40.194°C
Δ 47.388°C
□ 52.184°C
Apparent Viscosity (kN−s/m²)
350
300
250
200
150
0.05
0.1
0.15
0.2
0.25
Apparent shear rate (s⁻¹)

(d)

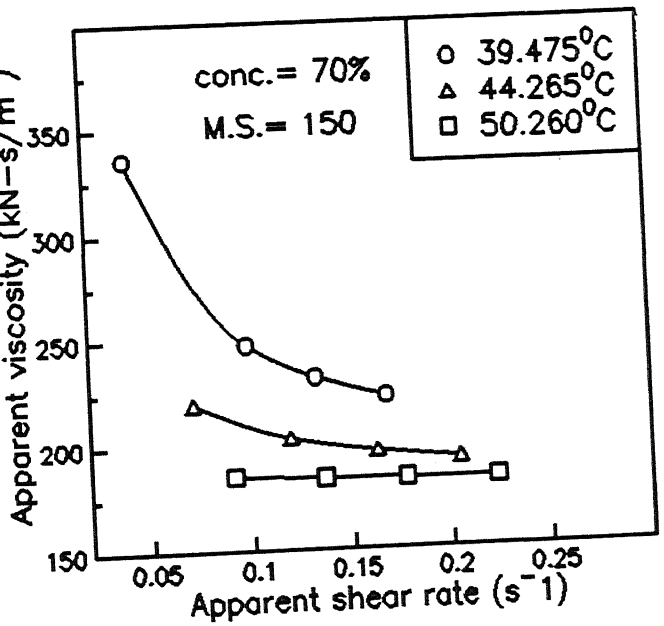
conc.= 70%
M.S.= 150
o 39.475°C
Δ 44.265°C
□ 50.260°C
Apparent viscosity (kN−s/m²)
350
300
250
200
150
0.05
0.1
0.15
0.2
0.25
Apparent shear rate (s⁻1)

(e)

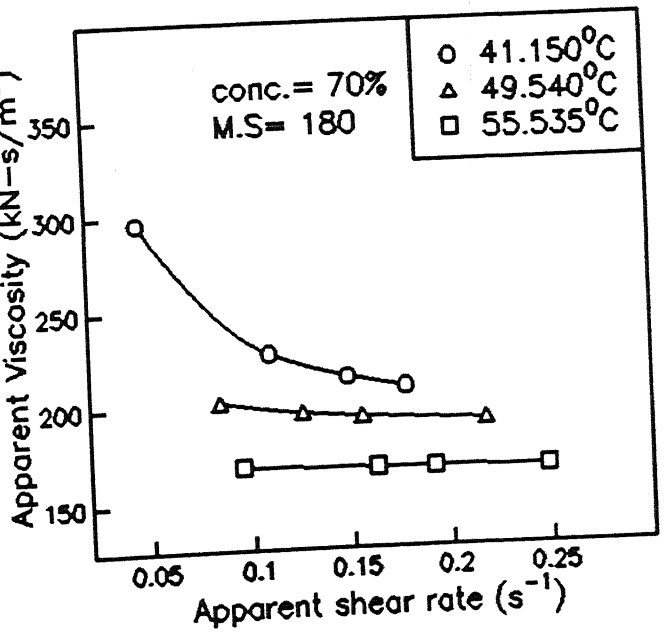
conc.= 70%
M.S= 180
o 41.150°C
Δ 49.540°C
□ 55.535°C
Apparent Viscosity (kN−s/m²)
350
300
250
200
150
0.05
0.1
0.15
0.2
0.25
Apparent shear rate (s⁻¹)

(f)

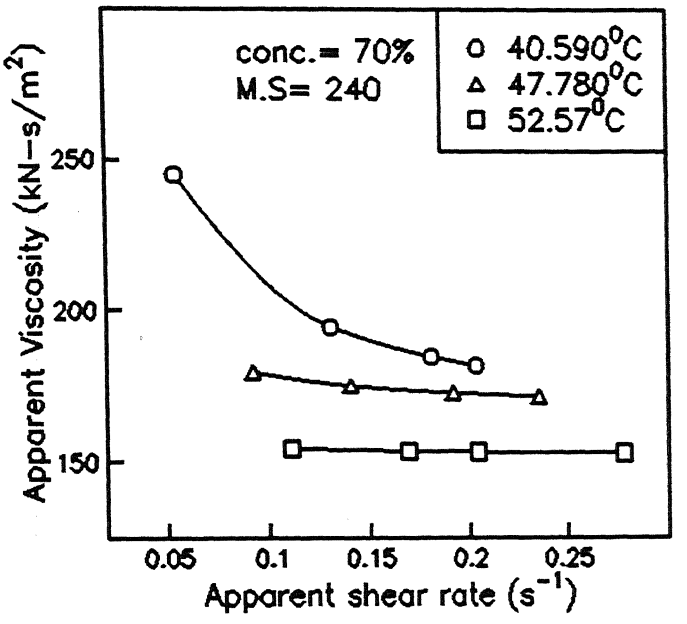

Fig. 4.6. Apparent shear rate v/s Apparent viscosity at different media temperatures

4.3 Effect of abrasive concentration

The experiments are conducted on a capillary viscometer set-up to determine the viscosity of the abrasive media at different concentrations. In Fig 4.1 graph is plotted between the average viscosity and concentrations at 50, 60, 70, 80% for varying mesh sizes 100,150,180. It is evident from the Fig. 4.7 that as the % concentration of abrasives increases in the media, the viscosity of the media increases. This can be explained as follows:

As the % concentration of the abrasives in the media increases, it decreases mobility of the particles migrating from the tube wall. Due to this, the amount of material extruded from the tube decreases as % concentration of the abrasives in the media increases which ultimately decreases volumetric flow rate ($\dot{Q}$) and the wall shear stress (because of decrease in pressure gradient p/L). And also, there is a decrease in apparent shear rate ($\dot{\gamma} = \frac{4\dot{Q}}{\pi r^3}$) due to the decrease in the volumetric flow rate. Due to this reason, there is an increase in the apparent viscosity($\eta_a = \eta_{pl} + \frac{\psi}{\dot{\gamma}}$) as the % concentration of abrasives in the media increases.

Table 4.1. Average apparent viscosities at different concentrations

Mesh size	Abrasive concentration (%)	Average apparent viscosity ($kN\text{-}s/m^2$)
100	50	378.760
	60	439.445
	70	541.724
	80	549.384
150	50	301.820
	60	368.559
	70	426.269
	80	472.114
180	50	260.749
	60	333.060
	70	371.537
	80	345.695

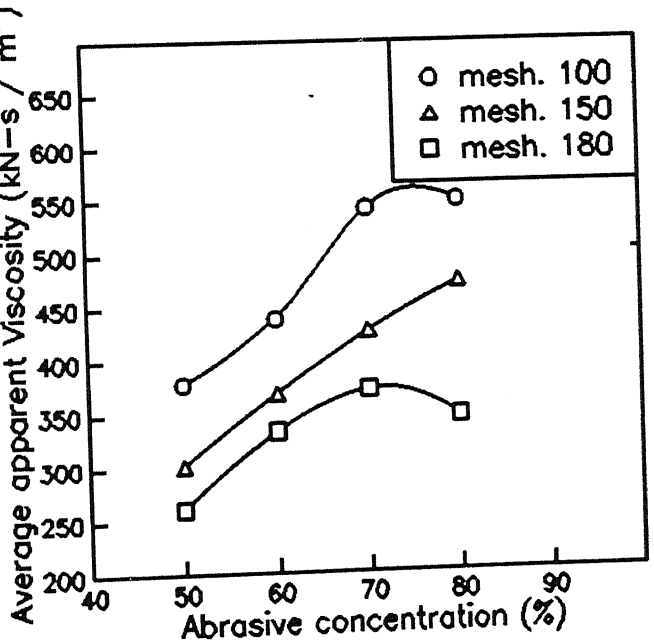

Fig 4.7 Effect of viscosity on abrasive concentration at room temperature

4.4 Effect of mesh size

The experiments are conducted at different mesh sizes to know the effect of mesh size on viscosity (average apparent viscosity). Fig 4.8 shows the graph plotted between the average viscosity and at different mesh sizes (100, 150, 180, 240) for concentration as 80%. From the Fig 4.8, it is evident that as the mesh size of abrasives increases (i.e. decrease in the grit size) the viscosity of the media decreases. This can be explained as follows.

As the mesh size increases, the amount of material extruded from the tube increases. As the amount of extruded material increases, the pressure gradient (p/L) and flow rate $\dot{Q}$ also increases. Due to this, there is an increase in apparent shear rate and wall shear stress. Due to this reason, there is decrease in the apparent viscosity of the media as the mesh size of the abrasives increases.

Table 4.2. Average apparent viscosities at different mesh sizes

Abrasive concentration (%)	Mesh size	Average apparent viscosity ($kN\text{-}s/m^2$)
80	100	549.384
	150	472.114
	180	345.695
	240	261.325

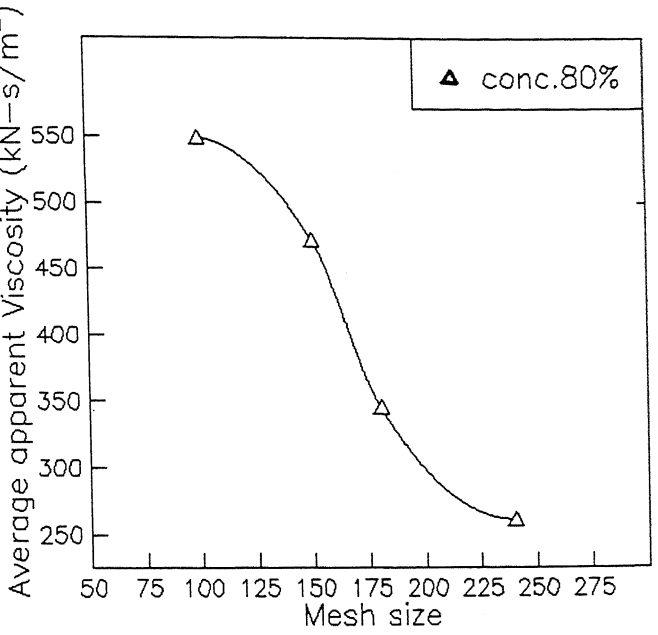

Fig 4.8. Effect of mesh size on viscosity at room temperature.

4.5 Effect of temperature

To study the effect of temperature on the viscosity, experiments are conducted at different concentrations and mesh sizes. Figs. 4.9(a,b) show the effect of media temperature on viscosity at different concentrations, and mesh sizes. From the Fig 4.9 (a,b), it is quite clear that as the temperature of the media increases, there is a decrease in the viscosity of the media. (The temperature of the media achieved is equal to the room temperature plus rise of temperature measured at inside periphery of the tube.)

This can be explained as follows;

As the temperature of the media increases there exists an increase in the flow rate (i.e an increase in extruded material) which causes increase in the apparent shear rate and increase in the wall shear stress (increase in the pressure gradient p/L). Due to this reason, viscosity of the media decreases as the temperature of the media increases.

Table 4.3(a) Average apparent viscosities at different concentrations and media temperatures

Mesh size	Abrasive concentration (%)	Media temperature (^{0}C)	Average apparent viscosity (kN-s/m^2)
100	50	37.515	216.641
		45.908	183.677
		53.102	151.820
	60	38.230	250.868
		44.225	203.640
		51.419	173.681
	70	40.194	292.335
		47.388	230.041
		52.184	199.814

Table 4.3(b) Average apparent viscosities at different mesh sizes and media temperatures

Abrasive concentration (%)	Mesh size	Media temperature (^{0}C)	Average apparent viscosity (kN-s/m^2)
70	100	40.194	292.335
		47.388	230.041
		52.184	199.814
	150	39.475	259.465
		44.265	202.865
		50.260	183.799
	180	41.150	236.840
		49.540	195.678
		55.535	166.874
	240	40.590	201.714
		47.780	174.823
		52.570	153.585

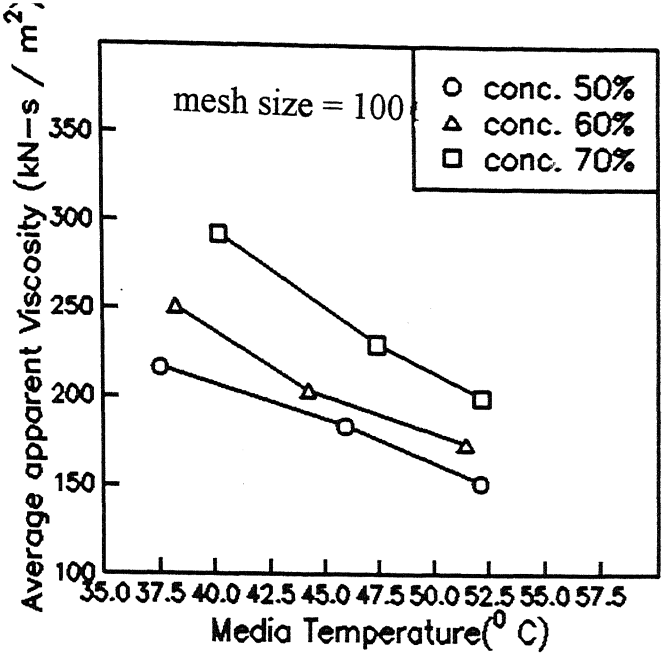

Fig 4.9(a) Effect of Media temperature on Viscosity at different concentrations

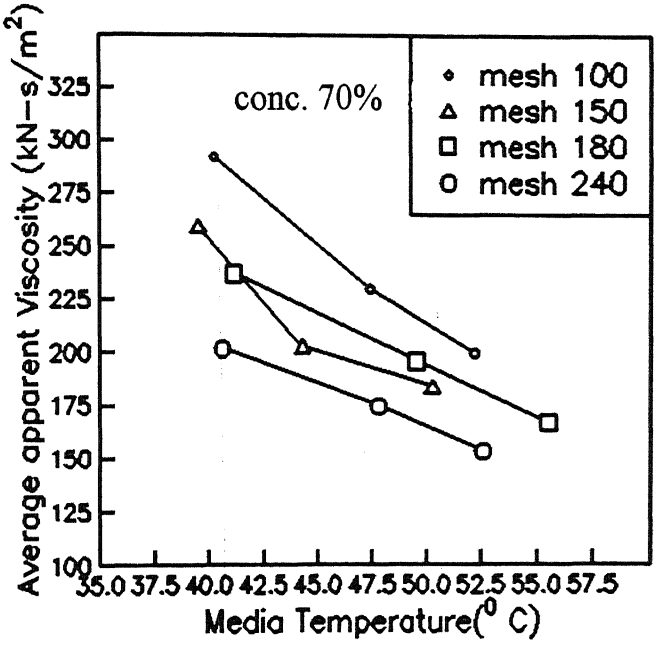

Fig 4.9(b) Effect of Media temperature on Viscosity at different mesh sizes.

4.6 Mathematical modelling by multi-variable analysis

The mathematical modelling is carried out with the help of multi-variable curve fitting technique. Using the multi-variable curve fitting technique for power law, the constants and powers of the regression equation for apparent viscosity are evaluated by computer program. Using the equation obtained from the regression analysis, the % errors between the experimental and theoretical values are calculated. The equation used for multi-variable analysis is given below:

$$y = a_0 x_1^{a_1} x_2^{a_2} x_3^{a_3}$$

Where, y = apparent viscosity and

a_0, a_1, a_2, a_3 = constants of regression.

x_1 = % concentration. by wt

x_2 = mesh size

x_3 = Temperature

4.6.1 Model for Viscosity

The constants of regression equation for the model are

$a_0 = 12229.86198$

$a_1 = 1.12862$

$a_2 = -0.46489$

$a_3 = -1.6986$

The regression equation for the curve is obtained as follows

$$y = 12229.86198\ x_1^{1.12862}\ x_2^{-0.46489}\ x_3^{-1.6986}$$

Using the above equation, theoretical values of viscosity and % error are calculated. All these values are given in table 1 in Appendix-II. From this

equation, it is clear that as the viscosity of the media increases as the % concentration increases, and it decreases with the increase in mesh size and temperature. To show the error between the theoretical and experimental values, the graphs are plotted at different concentrations, mesh sizes and temperatures as shown in Figs. 4.10 (a-b) and Fig. 4.11 (a-e).

(a)

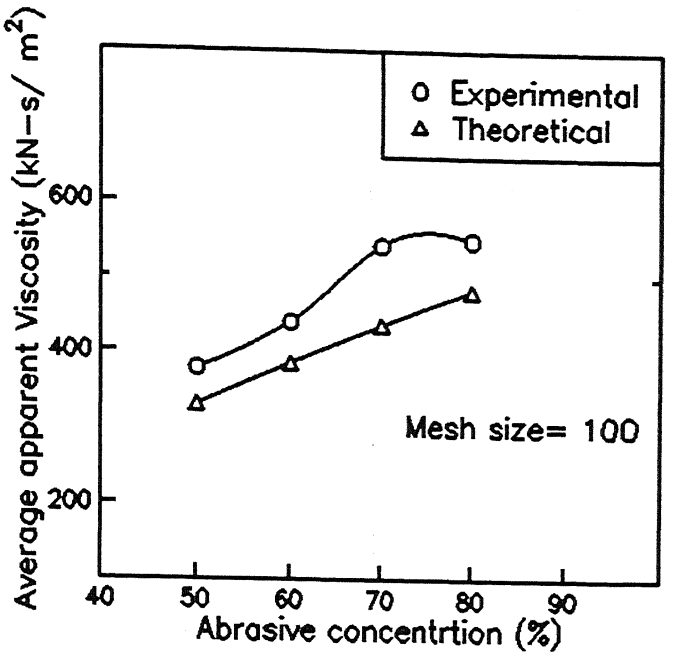

(b)

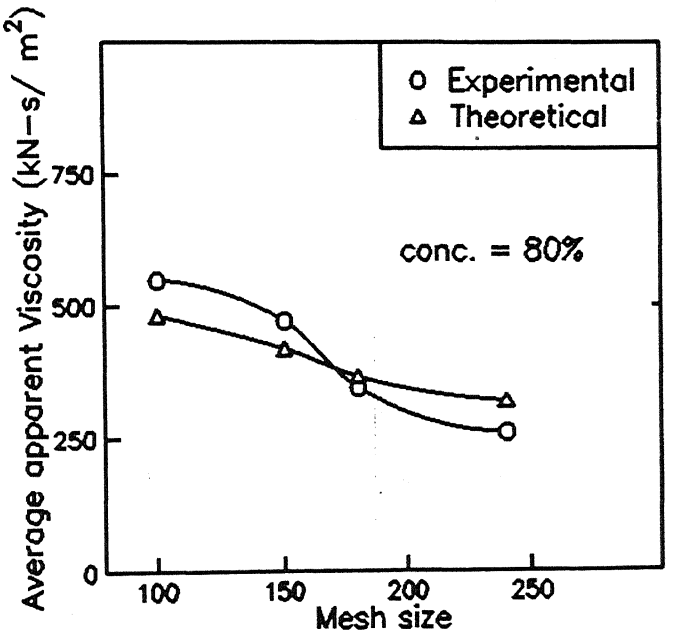

Fig 4.10 Comparison of Experimental and Theoretical results of viscosity at room temperature

(a)

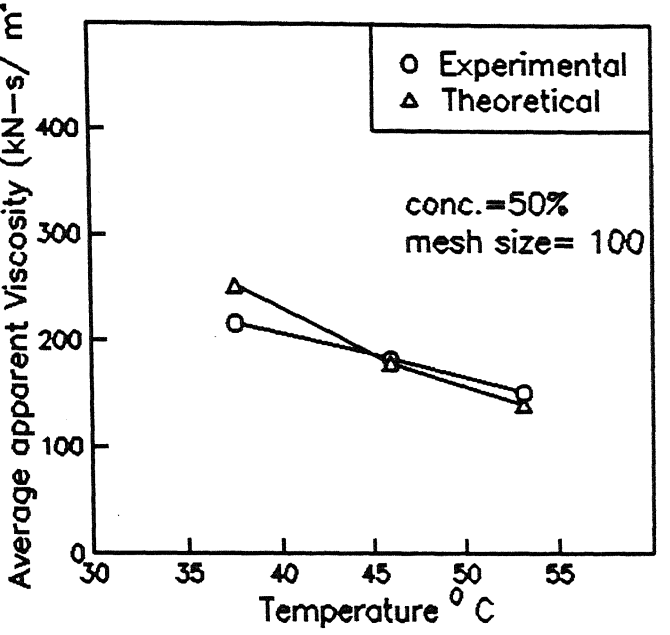
o Experimental
Δ Theoretical
conc.=50%
mesh size= 100
Average apparent Viscosity (kN-s/ m²)
0
100
200
300
400
30
35
40
45
50
55
Temperature ⁰C

(b)

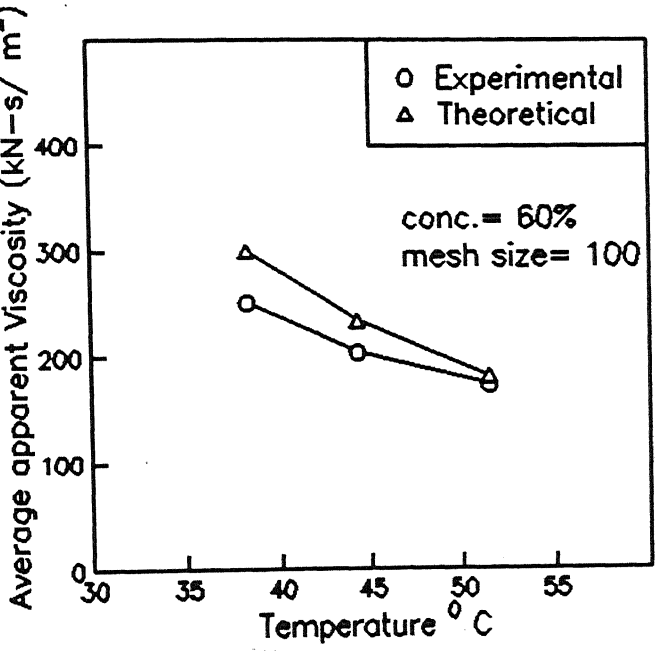
o Experimental
Δ Theoretical
conc.= 60%
mesh size= 100
Average apparent Viscosity (kN-s/ m²)
0
100
200
300
400
30
35
40
45
50
55
Temperature ⁰C

(c)

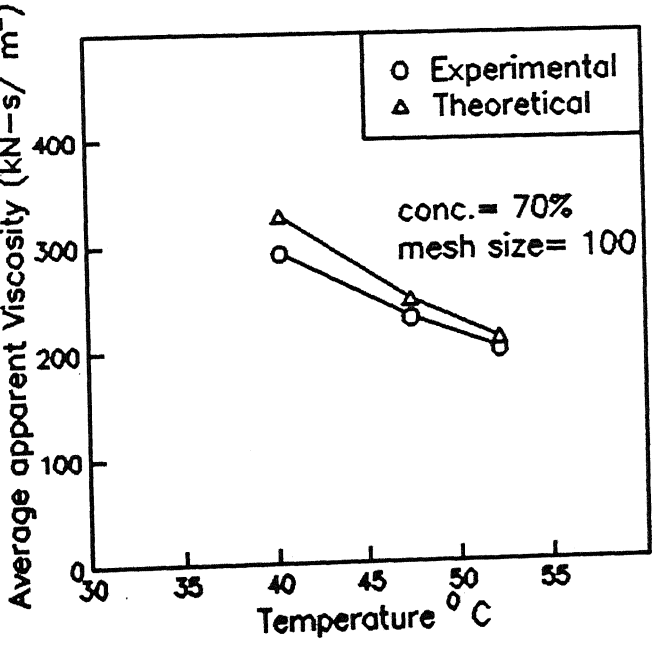
o Experimental
Δ Theoretical
conc.= 70%
mesh size= 100
Average apparent Viscosity (kN-s/ m²)
0
100
200
300
400
30
35
40
45
50
55
Temperature ⁰C

(d)

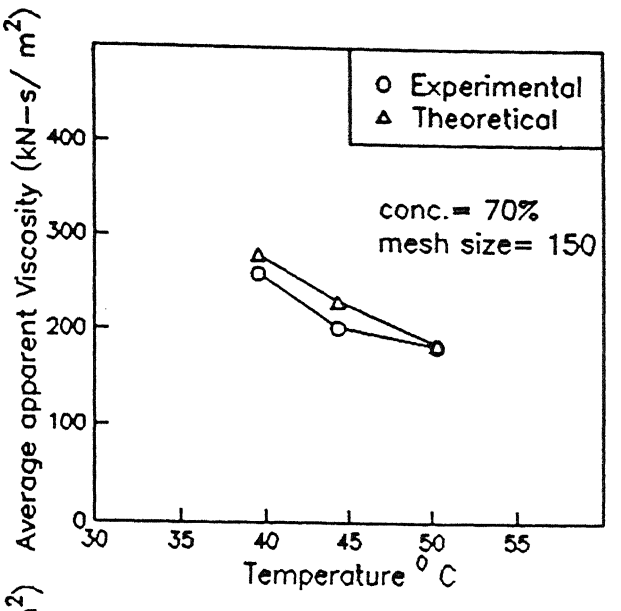

(e)

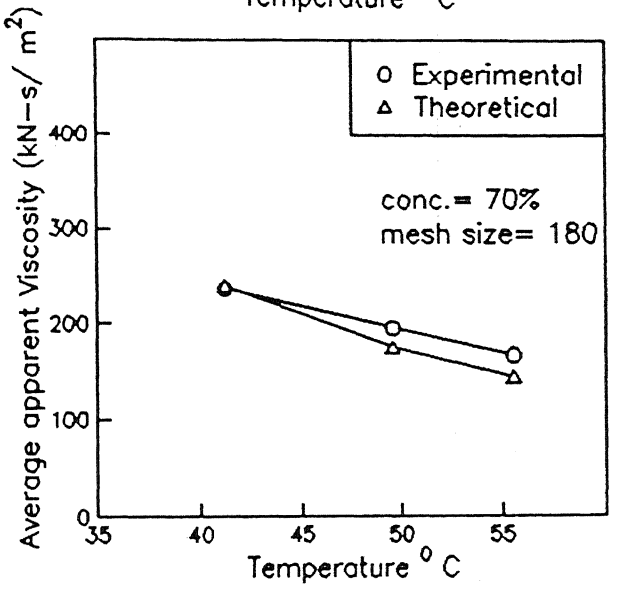

(f)

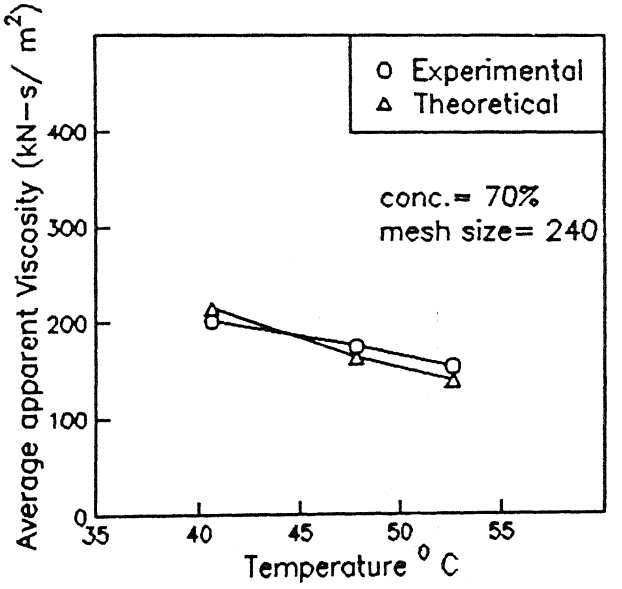

Fig 4.11 Comparison theoretical and Experimental results of viscosity at different media temperatures

4.7 Effect of viscosity on AFM process performance

From the literature review [Adsul 1996] it is observed that the process performance parameters, i.e. material removal and surface finish are significantly effected by abrasive concentration, grain size and media viscosity. It has been observed from the results reported in the previous sections that the viscosity of the media changes with the abrasive concentration and mesh size.

4.7.1 Effect of viscosity on MRR

Fig.4.12 (a,b) shows that as the viscosity of the media increases there is a consistent increase in material removal rate for both the materials, i.e aluminium and brass. This can be explained as follows:

As the viscosity of the media increases, there is an increase in the stiffness of the media, i.e it offers more resistance to the flow through the restriction (i.e.workpiece), which decreases the media flow rate. Due to more resistance between the abrasive grains and the surface to be machined, more abrasion takes place. Due to this, there is an increase in the cumulative material removal rate per cycle as the viscosity of the media increases.

Table 4.4(a) Material removal rate at different concentrations for 80 cycles [Adsul* ,1996]

Mesh size	Abrasive concentration (%)	Average apparent Viscosity (kN-s/m^2)	Material* removal rate for brass x10^{-4} (g)	Material* removal rate for aluminium x10^{-4} (g)
100	50	378.760	12.0	13.0
	60	439.445	20.0	23.0
	70	541.724	28.0	39.0
	80	549.384	29.0	38.0

Table 4.4(b) Material removal rate at different mesh sizes for 50 cycles[Adsul* , 1996]

Abrasive concentration (%)	Mesh size	Average apparent viscosity (kN-s/m^2)	Material* removal rate for brass x10^{-4} (g)	Material* removal rate for aluminium x10^{-4} (g)
80	100	549.384	18	23
	150	472.114	13	19
	180	345.695	13	14
	240	261.325	9	12

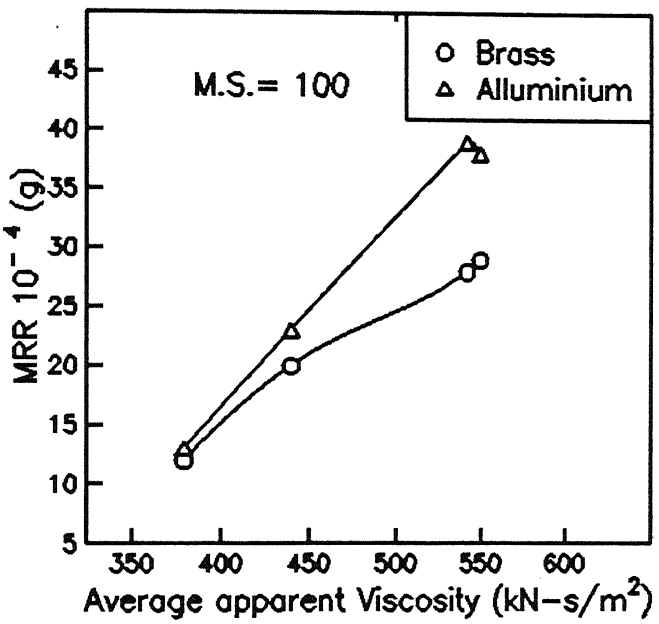

Fig. 4.12(a) Effect of viscosity on material removal rate

[Change in viscosity achieved by changing abrasive concentration.]

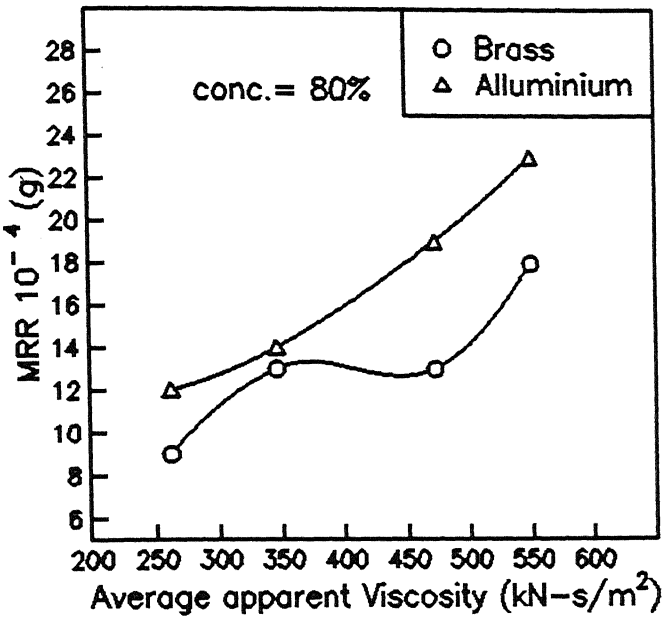

Fig. 4.12(b) Effect of viscosity on material removal rate
[change in viscosity achieved by changing mesh size]

4.7.2 Effect of viscosity on Surface Roughness

From the Figs 4.13 and 4.14 it is observed that as the viscosity of media increases there is a decrease in surface roughness values. This can be explained as follows:

The viscosity of the media increases when the % of concentration of abrasives increases in the media. Due to this, there is a decrease in the flow rate and shear rate. Due to increase in the stiffness of the abrasive media, it offers more resistance to the media flow through the restriction. Due to this, depth of penetration of abrasive grains in contact with the surface to be machined is more during machining which causes improvement in surface finish as the viscosity of the media increases.

Table 4.5 Surface roughness values at different concentrations at 80 cycles [Adsul* , 1996]

Mesh size	Abrasive concentration (%)	Average Viscosity (kN-s/m^2)	Surface roughness R_a ave. for brass* (μm)	Surface roughness R_a ave. for Aluminium* (μm)
100	50	378.760	16.34	1.48
	60	439.445	15.84	1.38
	70	541.724	15.12	0.90
	80	549.384	15.16	1.20

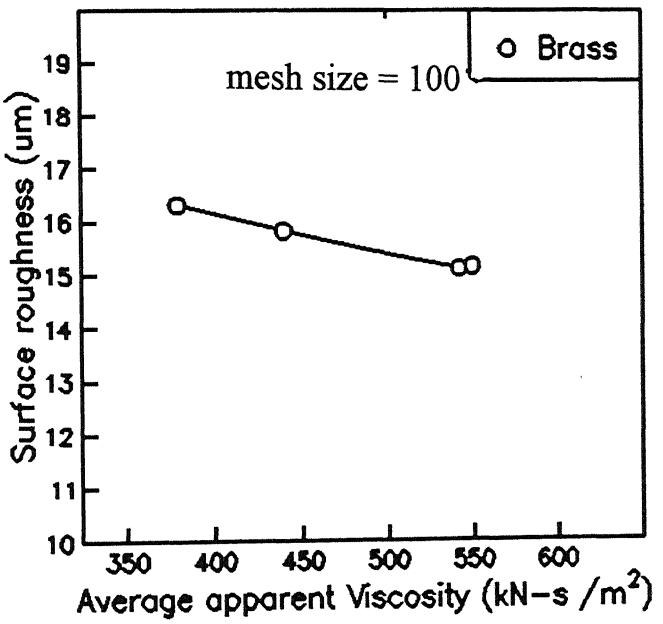

Fig 4.13 Effect of viscosity on Surface roughness for brass

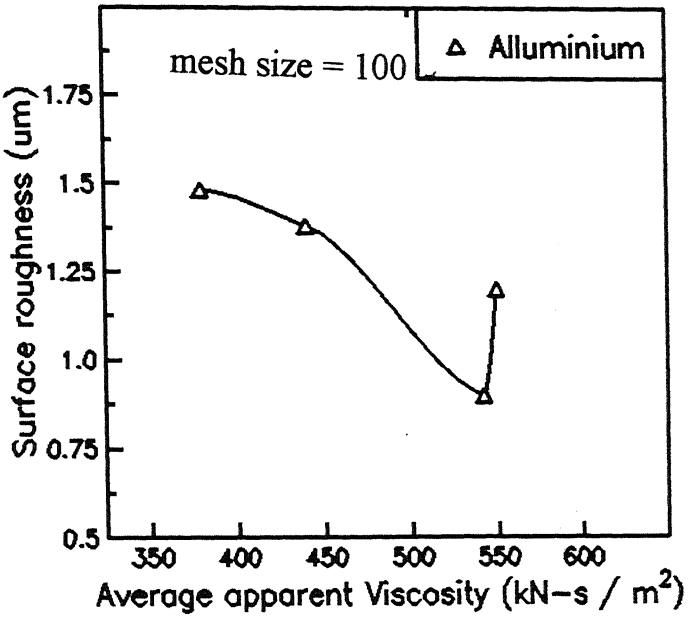

Fig 4.14 Effect of viscosity on Surface roughness for Aluminium

Chapter 5

CONCLUSIONS AND SCOPE FOR FUTURE WORK

5.1 Conclusions

The experiments are carried out to study the effects of abrasive concentration, mesh size and temperature on viscosity using capillary viscometer. These results are correlated with the process performance parameters, i.e material removal and surface finish and the following conclusions have been derived:

1. The viscosity of the media decreases with the increase in the shear rate and shear stress at the wall.
2. As the % concentration of the abrasives increases, there is a continuous increase in the viscosity of the media.
3. The viscosity of the media decreases with the increase in the mesh size (decrease in the grit size).
4. With the increase in the viscosity of the media, there is a consistent increase in the material removal for brass as well as aluminum.
5. With the increase in the viscosity of the abrasive media, there is a decrease in the surface roughness value.
6. From the mathematical model, it is found that the most dominating parameter is % concentration followed by the mesh size and temperature.
7. The apparent viscosity function was found to be a constant w.r.t to shear rate at the highest temperature range studied.

5. 2 Scope for the future work

1.There is a need to develope a mechanical device for efficient and mixing of abrasive grains in the media.

2. Investigations in the area of distribution of grains in mixture is require

3. Optimization of process parameters is needed to have better understa the process.

4. Repeatability of the data presented must be carefully established.

REFERENCES

Adsul S.G. - " Experimental investigations into Abrasive Flow Machining (AFM) at low pressure", M.Tech thesis, IIT Kanpur, 1996.

Christopher W. Macosko - " Rheology principles, Measurements, and applications", VCH Publishers Inc., 1994.

Davies P.J and Fletcher A.J., - "Assessment of rheological characteristics of abrasive flow machining process", Proc. Inst. Mech. Engrs., vol. 209, pp 409- 418, 1996.

Fletcher A.J. and Fioravanti A., - " Polishing and honing process: an investigation of thermal properties of mixtures of polyborosiloxane and silicon carbide", Proc. Inst. Mech. Engrs., vol. 210, pp 255-265,1996.

Ghosh A. and Mallik A.K. - " Manufacturing science", EWP Ltd., New Delhi, pp 269, 1985.

Insak et al.- " Abrasive flow machining in future", Annals of CIRP vol.42., pp 723, 1993.

Kohut Tom- "Surface finishing with abrasive flow machining", SME technical paper, pp 35-43, 1989.

Lee J. and Malkin S. - " Experimental investigations of the bore honing process ", Trans. ASME, Journal of Engg. for Ind., vol.115, pp 406, 1993.

Loveless T.R., Williams R.E. and Rajurkar K.P. - " A study of the effects of abrasive flow machining on various machined surfaces", Journal of material processing technology, vol 47, pp 133-151, 1994.

Malkin - " Grinding Technology - Theory and applications of machining with abrasives" John wiley sons, pp 19-20, 1989.

Onchi Y. and Mastumori N. - " Porous fine CBN stones for high removal rate superfinishing", Annals of CIRP, vol. 44, pp 291-294, 1995.

Perry - "Abrasive flow machining-principles and practices", Non-traditional conference proceedings (special report-private communication), pp 121-127, 1989.

Przylenk K. - " Abrasive flow machining - A process for surface finishing and deburring of workpiece with a complicated shape by means of an abrasive laden medium", Trans. ASME, PED vol. 22, pp 101-110, 1986.

Rajeshwar G., Kozak J.,and Rajurkar K.P., -"Modelling and simulation of Abrasive flow machining process", Proc. of Int. Mech. Engg conference, chicago, pp 1-7,1994 .

Rhoades L.J. - "Abrasive flow machining and its use", Non-traditional machining conference proceedings (special report) pp 111-120, 1989.

Rhoades L.J. - " Abrasive flow machining", Manufacturing Engg., pp 75-78, 1989.

Ronald Darby, - "Viscoelastic fluids", Marcel Dekkar Inc., pp 60-65, 1976.

Van Wazer - " Viscosity and flow measurement ", Interscience publishers, pp 189-191, 1963.

Williams R.E. and Rajurkar K.P. -" Stochastic modelling and analysis of abrasive flow machining.", Trans ASME, Journal of Engg. for Ind., vol. 14, pp 74-81, 1992.

Williams R.E and Rajurkar K.P., - "Metal removal and Surface finish characteristics in Abrasive flow machining"., Trans. ASME, PED vol 38, pp 93-106, 1989.

APPENDIX - I

1.1 Effect of mesh size on viscosity for various concentrations

To study the effect of abrasive concentration on viscosity the experiments are conducted at concentrations 50%, 60%, 70% for mesh sizes 100,150,180. The calulated values of viscosity are given in the following tables.

Table 1(a) Abrasive concentration = 50% Mesh size = 100

Room temperature =32^{0}C Yield stress ψ = 5.738 kN/m^2

Plastic viscosity η_{pl} = 265.139 kN-s/m^2

Weight w (kg)	Extruded length (m)	Average Length of the media $\bar{L}$ (m)	Apparent shear rate, $\dot{\gamma}$ (s^{-1})	Wall shear stress τ_w (kN/m^2)	Apparent viscosity η_a (kN-s/m^2)
23.7	0.0120	0.4740	0.034	16.788	433.918
28.7	0.0170	0.4715	0.048	20.437	384.690
33.7	0.0225	0.4688	0.064	24.138	354.803
38.7	0.0265	0.4667	0.075	27.838	341.652

Table 1(b) Abrasive concentration = 50% Mesh size = 150

Room temperature = 34 ^{0}C Yield stress ψ = 5.463 kN/m^2

Plastic viscosity η_{pl} = 215.632 kN-s/m^2

Weight w (kg)	Extruded length (m)	Average Length of the media $\bar{L}$ (m)	Apparent shear rate $\dot{\gamma}$ (s^{-1})	Wall shear stress τ_w (kN/m^2)	Apparent viscosity η_a (kN-s/m^2)
23.7	0.0145	0.4728	0.041	16.832	348.868
28.7	0.0225	0.4688	0.064	20.557	300.987
33.7	0.0295	0.4653	0.084	24.320	280.664
38.7	0.0325	0.4638	0.092	28.018	275.009

Table 1(c) Abrasive concentration = 50% Mesh size = 180

Room temperature = 34^{0}C Yield stress ψ= 5.17 kN/m^2

Plastic viscosity η_{pl}= 191.345 kN-s/m^2

Weight w (kg)	Extruded length (m)	Average length of the media $\bar{L}$ (m)	Apparent shear rate $\dot{\gamma}$ (s^{-1})	Wall shear stress τ_w (kN/m^2)	Apparent viscosity η_a (kN-s/m^2)
23.7	0.0170	0.4715	0.048	16.877	299.053
28.7	0.0275	0.4663	0.078	20.667	257.627
33.7	0.0325	0.4638	0.092	24.398	247.540
38.7	0.0385	0.4608	0.109	28.201	238.776

Table 2(a) Abrasive concentration = 60% Mesh size = 100

Room temperature = 33 ^{0}C Yield stress ψ = 6.898 kN/m^2

Plastic viscosity η_{pl} = 275.832 kN-s/m^2

Weight w (kg)	Extruded length (m)	Average Length of the media $\bar{L}$ (m)	Apparent shear rate $\dot{\gamma}$ (s^{-1})	Wall shear stress τ_w (kN/m^2)	Apparent viscosity η_a (kN-s/m^2)
23.7	0.0095	0.4753	0.027	16.743	531.320
28.7	0.0145	0.4728	0.041	20.383	444.082
33.7	0.0190	0.4705	0.054	24.048	403.577
38.7	0.0235	0.4683	0.067	27.749	378.791

Table 2(b) Abrasive concentration = 60% Mesh size = 150

Room temperature = 34^{0}C Yield stress ψ = 6.801 kN/m^2

Plastic viscosity η_{pl} = 234.417 kN-s/m^2

Weight w (kg)	Extruded length (m)	Average Length of the media $\bar{L}$ (m)	Apparent shear rate $\dot{\gamma}$ (s^{-1})	Wall shear stress τ_w (kN/m^2)	Apparent viscosity η_a (kN-s/m^2)
23.7	0.0115	0.4742	0.033	16.779	440.518
28.7	0.0175	0.4712	0.050	20.448	370.443
33.7	0.0215	0.4692	0.061	24.112	345.914
38.7	0.0290	0.4655	0.082	27.913	317.360

Table 2(c) Abrasive concentration = 60% Mesh size = 180

Room temperature = 33 ^{0}C Yield stress ψ = 6.058 kN/m^2

Plastic viscosity η_{pl} = 227.718 kN-s/m^2

Weight w (kg)	Extruded length (m)	Average Length of the media $\bar{L}$ (m)	Apparent shear rate $\dot{\gamma}$ (s^{-1})	Wall shear stress τ_w (kN/m^2)	Apparent viscosity η_a (kN-s/m^2)
23.7	0.0140	0.4730	0.040	16.823	379.174
28.7	0.0195	0.4703	0.055	20.491	337.868
33.7	0.0230	0.4685	0.065	24.151	320.922
38.7	0.0320	0.4640	0.091	28.003	294.292

Table 3(a) Abrasive concentration = 70% Mesh size = 100

Room temperature = 34 ^{0}C Yield stress ψ = 7.212kN/m^2

Plastic viscosity η_{pl} = 327.761 kN-s/m^2

Weight w (kg)	Extruded length (m)	Average Length of the media $\bar{L}$ (m)	Apparent shear rate $\dot{\gamma}$ (s^{-1})	Wall shear stress τ_w (kN./m^2)	Apparent viscosity η_a (kN-s/m^2)
23.7	0.0075	0.4762	0.021	16.708	671.212
28.7	0.0115	0.4742	0.033	20.318	546.321
33.7	0.0160	0.4720	0.045	23.972	488.038
38.7	0.0190	0.4705	0.054	27.616	461.325

Table 3(b) Abrasive concentration = 70% Mesh size = 150

Room temperature = 34 ^{0}C Yield stress ψ= 6.996 kN./m^2

Plastic viscosity η_{pl} = 266.308 kN-s/m^2

Weight w (kg)	Extruded length (m)	Average Length of the media $\bar{L}$ (m)	Apparent shear rate $\dot{\gamma}$ (s^{-1})	Wall shear stress τ_w (kN./m^2)	Apparent viscosity η_a (kN-s/m^2)
23.7	0.0105	0.4748	0.030	16.761	499.522
28.7	0.0140	0.4730	0.041	20.372	441.218
33.7	0.0185	0.4708	0.052	24.036	400.855
38.7	0.0255	0.4672	0.077	27.809	363.480

Table 3(c) Abrasive concentration = 70% Mesh size = 180

Room temperature = 34 ^{0}C Yield stress ψ= 7.239 kN./m^2

Plastic viscosity η_{pl} = 226.977 kN-s/m^2

Weight w (kg)	Extruded length (m)	Average Length of the media $\bar{L}$ (m)	Apparent shear rate $\dot{\gamma}$ (s^{-1})	Wall shear stress τ_w (kN/m^2)	Apparent viscosity η_a (kN-s/m^2)
23.7	0.0125	0.4737	0.035	16.796	433.827
28.7	0.0155	0.4723	0.044	20.404	391.517
33.7	0.0210	0.4695	0.057	24.100	347.640
38.7	0.0295	0.4653	0.077	27.928	313.165

Table 4 (a) Abrasive concentration = 80% Mesh size = 100

Room temperature = 35 ^{0}C Yield stress ψ = 7.6435 kN./m^2

Plastic viscosity η_{pl}= 316.752 kN-s/m^2

Weight w (kg)	Extruded length (m)	Average Length of the media $\bar{L}$ (m)	Apparent shear rate $\dot{\gamma}$ (s^{-1})	Wall shear stress τ_w (kN./m^2)	Apparent viscosity η_a (kN.-s/m^2)
23.7	0.0070	0.4565	0.020	16.699	698.928
28.7	0.0115	0.4743	0.033	20.318	548.374
33.7	0.0150	0.4725	0.043	23.947	494.508
38.7	0.0195	0.4703	0.055	27.631	455.725

Table 4(b) Abrasive concentration = 80% Mesh size = 150

Room temperature = 34 ^{0}C Yield stress ψ = 6.744 kN/m^2

Plastic viscosity η_{pl} = 301.87kN-s/m^2

Weight w (kg)	Extruded length (m)	Average Length of the media $\bar{L}$ (m)	Apparent shear rate $\dot{\gamma}$ (s^{-1})	Wall shear stress τ_w (kN./m^2)	Apparent viscosity η_a (kN-s/m^2)
23.7	0.0095	0.4753	0.027	16.743	551.674
28.7	0.0130	0.4735	0.037	20.351	484.159
33.7	0.0165	0.4718	0.047	23.985	445.374
38.7	0.0225	0.4688	0.064	27.719	407.256

Table 4(c) Abrasive concentration = 80% Mesh size = 180

Room temperature = 35 ^{0}C Yield stress ψ = 5.294 kN./m^2

Plastic viscosity η_{pl} = 251.640 kN-s/m^2

Weight w (kg)	Extruded length (m)	Average Length of the media $\bar{L}$ (m)	Apparent shear rate $\dot{\gamma}$ (s^{-1})	Wall shear stress τ_w (kN/m^2)	Apparent viscosity η_a (kN-s/m^2)
23.7	0.0140	0.4730	0.040	16.823	383.998
28.7	0.0185	0.4708	0.052	20.470	353.454
33.7	0.0235	0.4683	0.067	24.164	330.660
38.7	0.0295	0.4653	0.084	27.928	314.667

Table 4(d) Abrasive concentration = 80% Mesh size = 240

Room temperature = 35 ^{0}C Yield stress ψ = 3.814 kN/m^2

Plastic viscosity η_{pl} = 212.155 kN.-s/m^2

Weight w (kg)	Extruded length (m)	Average Length of the media $\bar{L}$ (m)	Apparent shear rate $\dot{\gamma}$ (s^{-1})	Wall shear stress τ_w (kN/m^2)	Apparent viscosity η_a (kN-s/m^2)
23.7	0.0205	0.4698	0.058	16.939	277.909
28.7	0.0250	0.4675	0.071	20.612	265.869
33.7	0.0315	0.4643	0.089	24.372	255.006
38.7	0.0390	0.4605	0.111	28.216	246.513

1.2 Effect of temperature on viscosity

To study the effect of temperature on viscosity of the media the experiments are conducted at concentrations 50%, 60%, 70% for a mesh sizes 100 and at mesh sizes 100,150,180,240 for a concentration 70%. The calculated values are given in the following tables.

Table.5(a) Abrasive concentration = 50% Mesh size = 100

Room temperature = 32^0C Initial water temperature= 31^0C

Temperature rise of water ΔT (^{0}C)	Voltage difference at side surface of tube (mV)	Voltage difference at the core of media (mV)	Temperature rise of media at side surface of tube (^{0}C)	Temperature rise of media at core (^{0}C)
10	0.23	0.15	5.515	3.59
20	0.35	0.30	13.908	10.784
30	0.30	0.15	21.102	14.374

---

* MT_S = Media temperature at side surface
  (Room temperature + Temperature rise of media)
* MT_C = Media temperature at core
  (Room temperature + Temperature rise of media)

Table 5(b) Abrasive conc. = 50% Mesh size = 100

$MT_s = 37.515^0C$ Yield stress $\psi = 4.370$ kN/m^2

$MT_c = 35.59^0C$ Plasticviscosity η_{pl}=175.775kN-s/m^2

Room temperature = 32^0C

Weight w (kg)	Extruded length (m)	Average Length of the media $\bar{L}$ (m)	Apparent shear rate $\dot{\gamma}$ (s^{-1})	Wall shear stress τ_w (kN/m^2)	Apparent viscosity η_a (kN-s/m^2)
23.7	0.0215	0.4692	0.061	16.957	247.414
33.7	0.0390	0.4605	0.111	24.571	215.144
43.7	0.0525	0.4538	0.149	32.336	205.104
53.7	0.0695	0.4453	0.197	40.494	197.958

Table 5(c) Abrasive conc.= 50% Mesh size = 100

$MT_s = 45.908^0C$ Yield stress ψ= 1.789 kN/m^2

$MT_c = 42.784^0C$ Plastic viscosity η_{pl}= 170.453 kN-s/m^2

Room temperature = 32^0C

Weight (w) kg	Extruded length (m)	Average Length of the media $\bar{L}$ (m)	Apparent shear rate $\dot{\gamma}$ (s^{-1})	Wall shear stress τ_w (kN/m^2)	Apparent viscosity η_a (kN-s/m^2)
23.7	0.0290	0.4655	0.082	17.094	192.274
33.7	0.0475	0.4563	0.135	24.800	183.707
43.7	0.0650	0.4475	0.185	32.787	180.178
53.7	0.0780	0.4410	0.221	40.884	178.549

Table 5(d) Abrasive conc. = 50% Mesh size = 100

$MT_S = 53.102\,^0C$ Yield stress $\psi = 1.435$ kN/m^2

$MT_C = 46.374^0C$ Plasticviscosity $\eta_{pl} = 143.262$kN-s/m^2

Room temperature = 32^0C

Weight w (kg)	Extruded length (m)	Average Length of the media $\bar{L}$ (m)	Apparent shear rate $\dot{\gamma}$ (s^{-1})	Wall shear stress τ_w (kN/m^2)	Apparent viscosity η_a (kN-s/m^2)
23.7	0.0370	0.4615	0.105	17.242	156.934
33.7	0.0580	0.4510	0.165	25.088	151.962
43.7	0.0770	0.4415	0.218	33.233	149.847
53.7	0.0980	0.4310	0.278	41.832	148.426

Table 6(a) Abrasive concentration 60% Mesh size = 100

Room temperature = 32^0C Initial water temperature = 30^0C

Temperature rise of water ΔT (^0C)	Voltage difference at side surface of the tube (mV)	Voltage difference at the core (mV)	Temperature rise of media at side surface (^0C)	Temperature rise of media at core (^0C)
10	0.26	0.13	6.23	3.117
20	0.25	0.15	12.225	6.714
30	0.30	0.25	19.419	12.709

Table 6(b) Abrasive conc = 60 % Mesh size = 100

$MT_s = 38.23^0$ C Yield stress $\psi = 6.817$ kN/m^2

$MT_c = 35.117^0$ C Plastic viscosity $\eta_{pl} = 169.25$kN-s/m^2

Room temperature = 32^0C

Weight (w) kg	Extruded length (m)	Average Length of the media $\bar{L}$ (m)	Apparent shear rate $\dot{\gamma}$ (s^{-1})	Wall shear stress τ_w (kN/m^2)	Apparent viscosity η_a (kN-s/m^2)
23.7	0.0140	0.4730	0.040	16.823	339.699
33.7	0.0355	0.4622	0.101	24.478	236.755
43.7	0.0470	0.4565	0.133	32.141	220.513
53.7	0.0645	0.4478	0.183	40.268	206.507

Table 6(c) Abrasive conc.= 60% Mesh size = 100

$MT_s = 44.225^0$ C Yield stress $\psi = 2.481$ kN/m^2

$MT_c = 38.714^0$ C Plastic viscosity $\eta_{pl} = 182.902$ kN-s/m^2

Room temperature = 32^0C

Weight w (kg)	Extruded length (m)	Average Length of the media $\bar{L}$ (m)	Apparent shear rate, $\dot{\gamma}$ (s^{-1})	Wall shear stress τ_w (kN/m^2)	Apparent viscosity η_a (kN-s/m^2)
23.7	0.0250	0.4675	0.071	17.021	217.841
33.7	0.0440	0.4580	0.125	24.705	202.748
43.7	0.0545	0.4527	0.155	32.407	198.906
53.7	0.0720	0.4440	0.204	40.608	195.062

Table 6(d) Abrasive conc. = 60% Mesh size = 100

$MT_S = 51.419^0C$ Yield stress $\psi = 0.6995$ kN/m^2

$MT_C = 44.709^0C$ Plastic viscosity $\eta_{pl} = 168.92$ kN-s/m^2

Room temperature = 32^0C

Weight w (kg)	Extruded length (m)	Average Length of the media $\bar{L}$ (m)	Apparent shear rate $\dot{\gamma}$ (s^{-1})	Wall shear stress τ_w (kN/m^2)	Apparent viscosity η_a (kN-s/m^2)
23.7	0.0320	0.4640	0.091	17.149	176.608
33.7	0.0525	0.4538	0.148	24.936	173.615
43.7	0.0670	0.4465	0.190	32.861	172.602
53.7	0.0830	0.4385	0.235	41.117	171.897

Table 7(a) Abrasive concentration = 70% Mesh size = 100

Room temperature= 33^0C Initial water temperature=32^0C

Temperature rise of water ΔT (^{0}C)	Voltage difference at side surface of the tube (mV)	Voltage difference at the core (mV)	Temperature rise of media at side surface (^{0}C)	Temperature rise of media at core (^{0}C)
10	0.30	0.23	7.194	5.515
20	0.30	0.25	14.388	9.510
30	0.20	0.15	19.184	13.107

Table 7(b) Abrasive conc. = 70% Mesh size = 100

$MT_s = 40.194^0$ C Yield stress $\psi = 6.205$ kN/m^2

$MT_c = 38.515^0$ C Plastic viscosity $\eta_{pl} = 205.496$ kN-s/m^2

Room temperature = 33^0C

Weight (w) kg	Extruded length (m)	Average Length of the media $\bar{L}$ (m)	Apparent shear rate $\dot{\gamma}$ (s^{-1})	Wall shear stress τ_w (kN/m^2)	Apparent viscosity η_a (kN-s/m^2)
23.7	0.0120	0.4740	0.034	16.788	387.997
33.7	0.0315	0.4642	0.089	24.372	275.215
43.7	0.0410	0.4595	0.116	31.931	258.987
53.7	0.0525	0.4538	0.149	39.735	247.141

Table 7(c) Abrasive conc = 70% Mesh size = 100

$MT_s = 47.388\ ^0$C Yield stress $\psi = 3.254$ kN/m^2

$MT_c = 42.510^0$ C Plastic viscosity $\eta_{pl} = 198.698$ kN-s/m^2

Room temperature = $33\ ^0$C

Weight w (kg)	Extruded length (m)	Average Length of the media $\bar{L}$ (m)	Apparent shear rate $\dot{\gamma}$ (s^{-1})	Wall shear stress τ_w (kN/m^2)	Apparent viscosity η_a (kN-s/m^2)
23.7	0.0220	0.4690	0.062	16.966	251.182
33.7	0.0355	0.4622	0.101	24.478	230.915
43.7	0.0515	0.4543	0.146	32.299	220.985
53.7	0.0625	0.4487	0.177	40.178	217.082

Table 7(d) Abrasive conc.= 70% Mesh size = 100

$MT_s = 52.184^0C$ Yield stress $\psi = 0.9265$ kN/m^2

$MT_c = 46.107^0$ C Plastic viscosity $\eta_{pl} = 192.530$ kN-s/m^2

Room temperature = 33^0C

Weight w (kg)	Extruded length (m)	Average Length of the media $\bar{L}$ (m)	Apparent shear rate $\dot{\gamma}$ (s^{-1})	Wall shear stress τ_w (kN/m^2)	Apparent viscosity η_a (kN-s/m^2)
23.7	0.0290	0.4655	0.082	17.094	203.829
33.7	0.0425	0.4588	0.121	24.664	200.187
43.7	0.0580	0.4510	0.165	32.533	198.145
53.7	0.0715	0.4442	0.203	40.585	197.094

Table 8 (a) Abrasive concentration = 70% Mesh size = 150

Room temperature = 33^0C Initial water temperature= 31^0C

Temperature rise of water ΔT (^{0}C)	Voltage difference at side surface of the tube (mV)	Voltage difference at the core (mV)	Temperature rise of media at side surface (^{0}C)	Temperature rise of media at core (^{0}C)
10	0.27	0.18	6.475	4.316
20	0.20	0.15	11.265	7.913
30	0.25	0.20	17.260	12.709

Table 8(b) Abrasive conc. = 70% Mesh size = 150

$MT_S = 39.475^0C$ Yield stress $\psi = 5.996$ kN/m^2

$MT_C = 37.316^0$ C Plastic viscosity $\eta_{pl} = 186.357$ kN-s/m^2

Room temperature = 33^0C

Weight w (kg)	Extruded length (m)	Average Length of the media $\bar{L}$ (m)	Apparent shear rate $\dot{\gamma}$ (s^{-1})	Wall shear stress τ_w (kN/m^2)	Apparent viscosity η_a (kN-s/m^2)
23.7	0.0140	0.4730	0.040	16.823	336.267
33.7	0.0345	0.4627	0.098	24.451	247.545
43.7	0.0465	0.4568	0.132	32.123	231.784
53.7	0.0590	0.4505	0.167	40.022	222.263

Table 8(c) Abrasive conc. = 70% Mesh size = 150

$MT_S = 44.265\ ^0C$ Yield stress $\psi = 2.969$ kN/m^2

$MT_C = 40.913^0$ C Plastic viscosity $\eta_{pl} = 177.950$ kN-s/m^2

Room temperature = 33^0C

Weight w (kg)	Extruded length (m)	Average Length of the media $\bar{L}$ (m)	Apparent shear rate $\dot{\gamma}$ (s^{-1})	Wall shear stress τ_w (kN/m^2)	Apparent viscosity η_a (kN-s/m^2)
23.7	0.0250	0.4675	0.071	17.021	219.772
33.7	0.0420	0.4590	0.119	24.651	202.903
43.7	0.0570	0.4515	0.162	32.497	196.279
53.7	0.0720	0.4440	0.204	40.608	192.506

Table 8(d) Abrasive conc. = 70% Mesh size = 150

$MT_s = 50.260^0C$ Yield stress $\psi = 0.3706$ KN/m^2

$MT_c = 45.709^0C$ Plastic viscosity $\eta_{pl} = 181.160$ KN-s/m^2

Room temperature = 33 ^{0}C

Weight w (kg)	Extruded length (m)	Average Length of the media $\bar{L}$ (m)	Apparent shear rate $\dot{\gamma}$ (s^{-1})	Wall shear stress τ_w (kN/m^2)	Apparent viscosity η_a (kN-s/m^2)
23.7	0.0320	0.4640	0.091	17.149	185.234
33.7	0.0480	0.4560	0.136	24.813	183.887
43.7	0.0625	0.4488	0.177	32.695	183.255
53.7	0.0785	0.4408	0.223	40.907	182.823

Table 9(a) Abrasive concentration= 70% Mesh size = 180

Room temperature =33^{0}C Initial water temperature = 32^{0}C

Temperature rise of water ΔT (^{0}C)	Voltage difference at side surface of the tube (mV)	Voltage difference at the core (mV)	Temperature rise of media at side surface (^{0}C)	Temperature rise of media at core (^{0}C)
10	0.34	0.28	8.150	6.71
20	0.35	0.20	16.540	11.506
30	0.25	0.15	22.535	15.103

Table 9(b) Abrasive conc. = 70% Mesh size = 180

$MT_S = 41.15\ ^0C$ Yield stress $\psi = 5.298\ kN/m^2$

$MT_C = 39.710\ ^0C$ Plastic viscosity $\eta_{pl} = 178.813\ kN\text{-}s/m^2$

Room temperature = 33^0C

Weight w (kg)	Extruded length (m)	Average Length of the media $\bar{L}$ (m)	Apparent shear rate $\dot{\gamma}$ (s^{-1})	Wall shear stress τ_w (kN/m^2)	Apparent viscosity η_a ($kN\text{-}s/m^2$)
23.7	0.0160	0.4720	0.045	16.859	296.565
33.7	0.0385	0.4608	0.109	24.557	227.426
43.7	0.0520	0.4540	0.148	32.318	214.616
53.7	0.0625	0.4487	0.177	40.178	208.750

Table9(c) Abrasive conc. = 70% Mesh size = 180

$MT_S = 49.54^0C$ Yield stress $\psi = 1.603 kN/m^2$

$MT_C = 44.506\ ^0C$ Plastic viscosity $\eta_{pl} = 183.272\ kN\text{-}s/m^2$

Room temperature = 33^0C

Weight w (kg)	Extruded length (m)	Average Length of the media $\bar{L}$ (m)	Apparent shear rate $\dot{\gamma}$ (/sec)	Wall shear stress τ_w (kN/m^2)	Apparent viscosity η_a ($kN\text{-}s/m^2$)
23.7	0.0295	0.4653	0.084	17.103	202.352
33.7	0.0440	0.4580	0.125	24.705	196.093
43.7	0.0545	0.4528	0.155	32.407	193.612
53.7	0.0765	0.4418	0.217	40.814	190.658

Table 9(d) Abrasive conc. = 70% Mesh size = 180

MT_s = 55.535 ^{0}C Yield stress ψ= 0.369 kN/m^2

MT_c = 48.103 ^{0}C Plastic viscosity η_{pl}= 164.478 kN-s/m^2

Room temperature = 33^{0}C

Weight w (kg)	Extruded length (m)	Average Length of the media $\bar{L}$ (m)	Apparent shear rate $\dot{\gamma}$ (/sec)	Wall shear stress τ_w (kN/m^2)	Apparent viscosity η_a (kN-s/m^2)
23.7	0.0335	0.4633	0.095	17.117	168.363
33.7	0.0570	0.4515	0.162	25.060	166.756
43.7	0.0675	0.4462	0192	32.879	166.410
53.7	0.0875	0.4363	0.248	41.329	165.966

Table 10(a)Abrasive concentration = 70% Mesh size = 240

Room temperature = 31^{0}C Initial water temperature= 32^{0}C

Temperature rise of water ΔT (^{0}C)	Voltage difference at side surface of the tube (mV)	Voltage difference at the core (mV)	Temperature rise of media at side surface (^{0}C)	Temperature rise of media at core (^{0}C)
10	0.40	0.31	9.59	7.43
20	0.30	0.15	16.78	11.027
30	0.20	0.15	21.57	14.624

Table 10(b) Abrasive conc. = 70% Mesh size = 240

$MT_S = 40.59\ ^0C$ Yield stress $\psi = 4.6624$ kN/m^2

$MT_C = 38.43\ ^0C$ Plastic viscosity $\eta_{pl} = 158.945$ kN-s/m^2

Room temperature = 31^{0}C

Weight w (kg)	Extruded length (m)	Average Length of the media $\bar{L}$ (m)	Apparent shear rate $\dot{\gamma}$ (s^{-1})	Wall shear stress τ_w (kN/m^2)	Apparent viscosity η_a (kN-s/m^2)
23.7	0.0190	0.4705	0.054	16.912	245.286
33.7	0.0460	0.4570	0.130	24.759	194.809
43.7	0.0635	0.4482	0.180	32.732	184.847
53.7	0.0715	0.4442	0.203	40.585	181.912

Table 10(c) Abrasive conc. = 70% Mesh size = 240

$MT_S = 47.78^0C$ Yield stress $\psi = 1.205$ kN/m^2

$MT_C = 42.027^0C$ Plastic viscosity $\eta_{pl} = 166.537$ kN-s/m^2

Room temperature =31^0 C

Weight w (kg)	Extruded length (m)	Average Length of the media $\bar{L}$ (m)	Apparent shear rate $\dot{\gamma}$ (s^{-1})	Wall shear stress τ_w (kN/m^2)	Apparent viscosity η_a (kN-s/m^2)
23.7	0.0325	0.4638	0.092	17.159	179.637
33.7	0.0495	0.4552	0.140	24.854	175.145
43.7	0.0670	0.4465	0.190	32.879	172.847
53.7	0.0830	0.4385	0.236	41.117	171.665

Table 10(d) Abrasive conc.= 70% Mesh size = 240

MT_s = 52.57 ^{0}C Yield stress ψ = 0.293 kN/m^2

MT_c = 45.624^0 C Plastic viscosity η_{pl}= 151.868 kN-s/m^2

Room temperature = 31^{0}C

Weight w (kg)	Extruded length (m)	Average Length of the media $\bar{L}$ (m)	Apparent shear rate $\dot{\gamma}$ (s^{-1})	Wall shear stress τ_w (kN/m^2)	Apparent viscosity η_a (kN-s/m^2)
23.7	0.0390	0.4605	0.111	17.280	154.510
33.7	0.0595	0.4502	0.169	25.130	153.604
43.7	0.0720	0.4440	0.204	33.046	153.306
53.7	0.0980	0.4310	0.278	41.832	152.923

Appendix - II

Table 2 Results of viscosity at various concentrations, mesh sizes and temperatures

% conc.	Mesh size	Temperature (^{0}C)	Experimental viscosity (kN-s/m^2)	Theoretical viscosity (kN-s/m^2)	% error
50	100	32.0	378.760	329.967	12.882
60	100	33.0	439.445	384.712	12.455
70	100	34.0	541.724	435.182	19.667
80	100	35.0	549.384	481.657	12.328
80	150	34.0	472.114	419.043	11.241
80	180	35.0	345.695	366.492	6.016
80	240	35.0	261.325	320.613	22.688
50	100	37.515	216.641	251.868	16.261
50	100	45.908	183.677	178.745	2.686
50	100	53.102	151.820	139.586	8.058
60	100	38.230	250.868	299.645	19.444
60	100	44.225	203.640	233.965	14.892
60	100	51.419	173.681	181.120	4.283
70	100	40.194	292.335	327.500	12.029
70	100	47.388	230.041	247.599	7.633
70	100	52.184	199.814	210.199	5.198
70	150	39.475	259.645	279.682	7.717
70	150	44.265	202.865	230.239	13.494
70	150	50.260	183.799	185.558	0.957
70	180	41.150	236.844	239.440	1.098
70	180	49.540	195.678	174.708	10.716
70	180	55.535	166.874	143.894	13.771
70	240	40.590	201.714	214.399	6.288
70	240	47.780	174.823	162.523	7.035
70	240	52.570	153.585	138.177	10.032

APPENDIX - III

Table 3. Typical values of viscosity of some familiar materials at room temperaraure [Christopher , 1994]

Material	Approximate Viscosity (Pa-s)
Glass	10^{48}
Molten glass(500^0 C)	10^{12}
Bitumen	10^{8}
Asphalt	10^{8}
Molten polymers	10^{3}
Heavy syrup	10^{2}
Honey	10^{1}
Glycerin	10^{0}
Olive oil	10^{-1}
Light oil	10^{-2}
Water	10^{-3}
Air	10^{-5}
Putty (present case)	10^{5}-10^{6}

Appendix - IV

4.1 Interpretation of Apparent viscosity

Generally, for Newtonian fluids η is the ratio of shear stress to the shear rate is called as viscosity. Since the ratio of the shear stress to the shear rate is not a constant (i.e. doubling the shear stress will not result in twice the shear rate and vice-versa), it defines a function so called the apparent viscosity of shear-dependent viscosity as

$$\eta_a(\dot{\gamma}) = \frac{\tau}{\dot{\gamma}}$$

Plastic viscosity(η_{pl}) is the ratio of the excess of shear stress over the yield stress divided by the rate of shear for a Bingham plastic material.

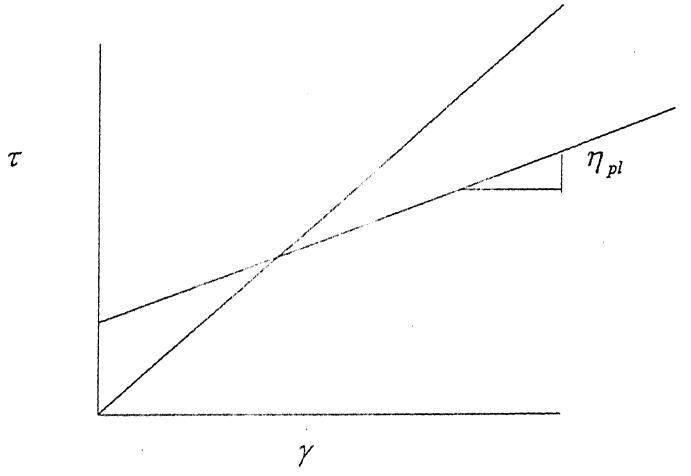

From the results, it is observed that the apparent viscosity is approaching approrximately the plastic viscosity as the shear rate increases.